Segmentation and Morphotectonic Variations Along a Slow-Spreading Center: The Mid-Atlantic Ridge (24°00′ N–30°40′ N)

JEAN-CHRISTOPHE SEMPÉRÉ[1], JIAN LIN[2], HOLLY S. BROWN[1], HANS SCHOUTEN[2], and G. M. PURDY[2]

[1]*School of Oceanography, University of Washington, Seattle, WA 98195, U.S.A.*
[2]*Department of Geology and Geophysics, Woods Hole Oceanographic Institution, Woods Hole, MA 02543, U.S.A.*

(Received 20 November, 1991; in final form 12 August, 1992)

Key words: Mid-Atlantic Ridge, bathymetry

Abstract. Analysis of Sea Beam bathymetry along the Mid-Atlantic Ridge between 24°00′ N and 30°40′ N reveals the nature and scale of the segmentation of this slow-spreading center. Except for the Atlantis Transform, there are no transform offsets along this 800-km-long portion of the plate boundary. Instead, the Mid-Atlantic Ridge is offset at intervals of 10–100 km by non-transform discontinuities, usually located at local depth maxima along the rift valley. At these discontinuities, the horizontal shear between offset ridge segments is not accommodated by a narrow, sustained transform-zone. Non-transform discontinuities along the MAR can be classified according to their morphology, which is partly controlled by the distance between the offset neovolcanic zones, and their spatial and temporal stability. Some of the non-transform discontinuities are associated with off-axis basins which integrate spatially to form discordant zones on the flanks of the spreading center. These basins may be the fossil equivalents of the terminal lows which flank the neovolcanic zone at the ends of each segment. The off-axis traces, which do not lie along small circles about the pole of opening of the two plates, reflect the migration of the discontinuities along the spreading center.

The spectrum of rift valley morphologies ranges from a narrow, deep, hourglass-shaped valley to a wide valley bounded by low-relief rift mountains. A simple classification of segment morphology involves two types of segments. Long and narrow segments are found preferentially on top of the long-wavelength, along-axis bathymetric high between the Kane and Atlantis Transforms. These segments are associated with circular mantle Bouguer anomalies which are consistent with focused mantle upwelling beneath the segment mid-points. Wide, U-shaped segments in cross-section are preferentially found in the deep part of the long-wavelength, along-axis depth profile. These segments do not appear to be associated with circular mantle Bouguer anomalies, indicating perhaps a more complex pattern of mantle upwelling and/or crustal structure. Thus, the long-recognized bimodal distribution of segment morphology may be associated with different patterns of mantle upwelling and/or crustal structure. We propose that the range of observed, first-order variations in segment morphology reflects differences in the flow pattern, volume and temporal continuity of magmatic upwelling at the segment scale. However, despite large first-order differences, all segments display similar intra-segment, morphotectonic variations. We postulate that the intra-segment variability represents differences in the relative importance of volcanism and tectonism along strike away from a zone of enhanced magma upwelling within each segment. The contribution of volcanism to the morphology will be more important near the shallowest portion of the rift valley within each segment, beneath which we postulate that upwelling of magma is enhanced, than beneath the ends of the segment. Conversely, the contribution of tectonic extension to the morphology will become more important toward the spreading center discontinuities. Variations in magmatic budget along the strike of a segment will result in along-axis variations in crustal structure. Segment mid-points may coincide with regions of highest melt production and thick crust, and non-transform discontinuities with regions of lowest melt production and thin crust. This hypothesis is consistent with available seismic and gravity data.

The rift valley of the Mid-Atlantic Ridge is in general an asymmetric feature. Near segment mid-points, the rift valley is usually symmetric but, away from the segment mid-points, one side of the rift valley often consists of a steep, faulted slope while the other side forms a more gradual ramp. These observations suggest that half-grabens, rather than full-grabens, are the fundamental building blocks of the rift valley. They also indicate that the pattern of faulting varies along strike at the segment scale, and may be a consequence of the three-dimensional, thermo-mechanical structure of segments associated with enhanced mantle upwelling beneath their mid-points.

1. Introduction

High-resolution mapping of the mid-ocean ridge system reveals that spreading centers can be divided into distinct accretionary segments separated by axial discontinuities. The segmentation of mid-ocean ridges is a fundamental phenomenon which reflects the three-dimensional nature of accretionary processes at divergent plate boundaries (e.g., Schouten and White, 1980; Schouten and Klitgord, 1982; Whitehead *et al.*, 1984; Crane, 1985). The characteristics of segmentation of the fast-spreading East Pacific Rise (EPR) have been intensively studied in

Marine Geophysical Researches **15**: 153–200, 1993.

recent years (e.g., Macdonald *et al.*, 1984, 1986; Lonsdale, 1983, 1985, 1989a, 1989b). Definition of the segmentation of the EPR has been facilitated by the relative ease of studying its narrow (<2–3 km) neovolcanic zone with swath-mapping systems. In contrast, because the locus of crustal accretion of the Mid-Atlantic Ridge (MAR) occurs within a wide (10–30 km) rift valley, defining the characteristics of segmentation of this slow-spreading center requires considerably more effort and time. As a result, although the segmentation of the MAR has been characterized in the South Atlantic (e.g., Vogt *et al.*, 1987; Brozena and Chayes, 1988; Fox *et al.*, 1991; Grindlay *et al.*, 1991; Carbotte *et al.*, 1991), it has remained poorly constrained in the North Atlantic. Available echo-sounding data indicate that the MAR is partitioned by closely-spaced (~50 km) offsets which disrupt the continuity of the axial rift valley, and which have morphologies distinct from that of large fracture zones (Johnson and Vogt, 1973; Rona, 1976; Searle and Laughton, 1977; Phillips and Fleming, 1977; Ramberg *et al.*, 1977; Rona and Gray, 1980). These offsets are characterized by oblique fault scarps in plan view with no evidence of sustained strike-slip motion. In some cases, these offsets are associated with off-axis traces which, unlike fracture zones, do not follow small circles about the pole of opening of the two plates. These features are typical of crustal accretion in the South Atlantic (Fox *et al.*, 1985; Brozena, 1986; Vogt *et al.*, 1987; 1988; Brozena and Chayes, 1988; Fox *et al.*, 1991; Grindlay *et al.*, 1991), but their nature and evolution have remained ill-defined in the North Atlantic.

Prior to this study, multibeam bathymetric coverage was only available in two areas along the MAR in the central North Atlantic: the FAMOUS and MARK areas (Phillips and Fleming, 1977; Karson *et al.*, 1987; Kong *et al.*, 1988). Although the FAMOUS and MARK area studies have greatly increased our understanding of slow-spreading centers, the length of along-axis coverage obtained during these studies has been insufficient to define the variability of accretionary processes along the MAR, and to provide strong constraints on models of these processes. Inferences about the evolution of the MAR have been made on the basis of individual echo-sounding profiles, often spaced by as much as several hundred km. However, widely-spaced profiles from spreading segments in different volcano-tectonic settings do not provide a faithful representation of the morphologic spectrum of the spreading center. In this study, we present some of the results of a geophysical investigation of an 800-km-long section of the MAR (24°00′–30°40′ N, Figure 1a) (Sempéré *et al.*, 1990). This paper focuses on the segmentation and morphotectonic characteristics of the spreading center. Although the data discussed in this paper further our understanding of the along-axis character of the MAR, they may not be representative of the entire spectrum of crustal accretion along this slow-spreading center (i.e., Needham *et al.*, 1991; Gente *et al.*, 1991), and they do not adequately constrain the evolution of the spreading center because of their limited across-axis extent.

2. Data Collection and Analysis

The data presented in this study were collected during a two-leg Sea Beam investigation of the Mid-Atlantic Ridge in September–October 1988 (RC 2909) and December 1988–January 1989 (RC 2912) aboard the R/V Robert D. Conrad. The spreading center between the western Kane ridge-transform intersection (~23°50′ N) and latitude 27°40′ N was mapped during leg 1, and the spreading center between 27°40′ N and 30°40′ N during leg 2. Magnetic data were collected on both legs, but gravity data were acquired only during leg 2. Coverage consisted of 50–75-km-long lines perpendicular to the spreading center (010°). Spacing of profiles varied between 2.0 and 3.3 km, depending on axial depth, to allow full coverage of the rift valley. About 50% coverage was obtained in the rift mountains.

Sea Beam is a multi-narrow-beam echo-sounder which can ensonify a swath of seafloor with a width of ~3/4 of the water depth (Glenn, 1976; Renard and Allenou, 1979). In the rough topography of the MAR, the vertical resolution of Sea Beam is on the order of 10–20 m (Tyce, 1986). Navigation was obtained by a combination of Transit satellites and the Global Positioning System (GPS). Because GPS was available less than 2 hours a day, most of the navigation is interpolated between Transit satellite fixes. Post-cruise processing involved the determination of the final ship navigation using the best available fixes (Transit and GPS), and the constraints imposed by crossing or overlapping Sea Beam swaths (Purdy *et al.*, 1990).

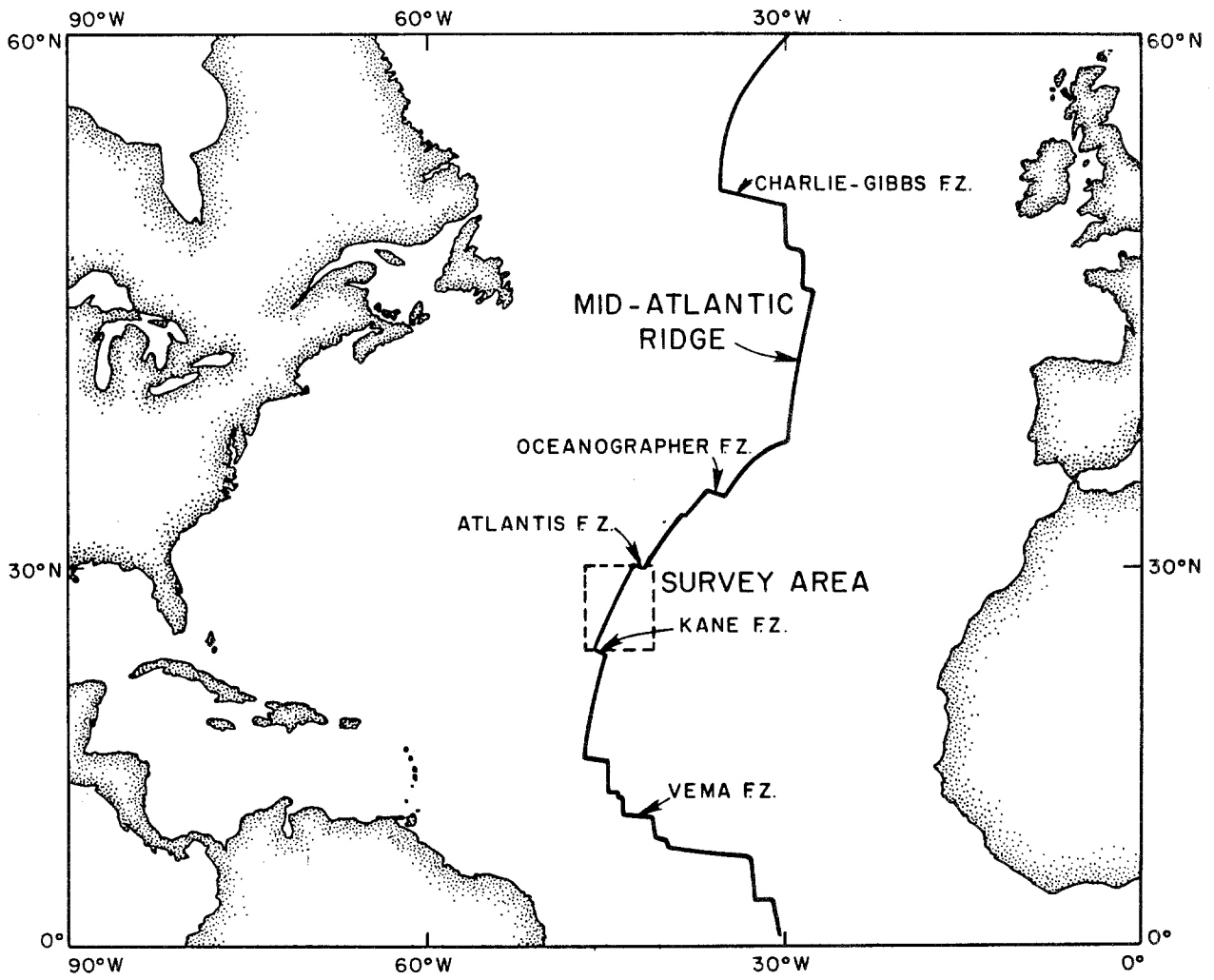

Fig. 1a. Location of the survey area.

We have interpreted Sea Beam bathymetric data in terms of the structural geomorphology of the MAR. In our interpretation very steep slopes with sub-linear strikes are assumed to be faults. The reader should bear in mind that it is difficult to distinguish between steep volcanic slopes and fault scarps on the basis of Sea Beam data alone. In the absence of sidescan sonar imagery or groundtruth information, the neovolcanic zone (NVZ), the zone of most recent volcanism, is interpreted as the sub-linear locus of bathymetric peaks, inferred to be of volcanic origin, found within the inner floor of the rift valley in each segment. When the NVZ lies on top of a narrow ridge, sub-parallel to the orientation of the rift valley, we refer to it as the neovolcanic ridge. The NVZ corresponds to a high in the magnetization distribution obtained by inverting the surface magnetic field over each segment (Sempéré *et al.*, in prep.). Since the most recent basalts are in general, but not always (e.g., Prévot *et al.*, 1979), the most highly magnetized, the magnetic results are in agreement with our morphotectonic determination of the locus of the NVZ. To help the reader assess the robustness of the NVZ, we have devised a simple classification of this feature. The NVZ is described as (1) robust where it consists of a linear ridge >200-m high which is studded by small, volcanic cones, (2) intermediate where it consists of a discontinuous ridge <200-m high formed by elongate, volcanic structures several km long, and (3) poorly-developed where it consists of a string of subcircular volcanic edifices.

The terms marginal, terminal and nodal basins describe bathymetric lows found within the rift valley. Marginal basins may occur anywhere within the

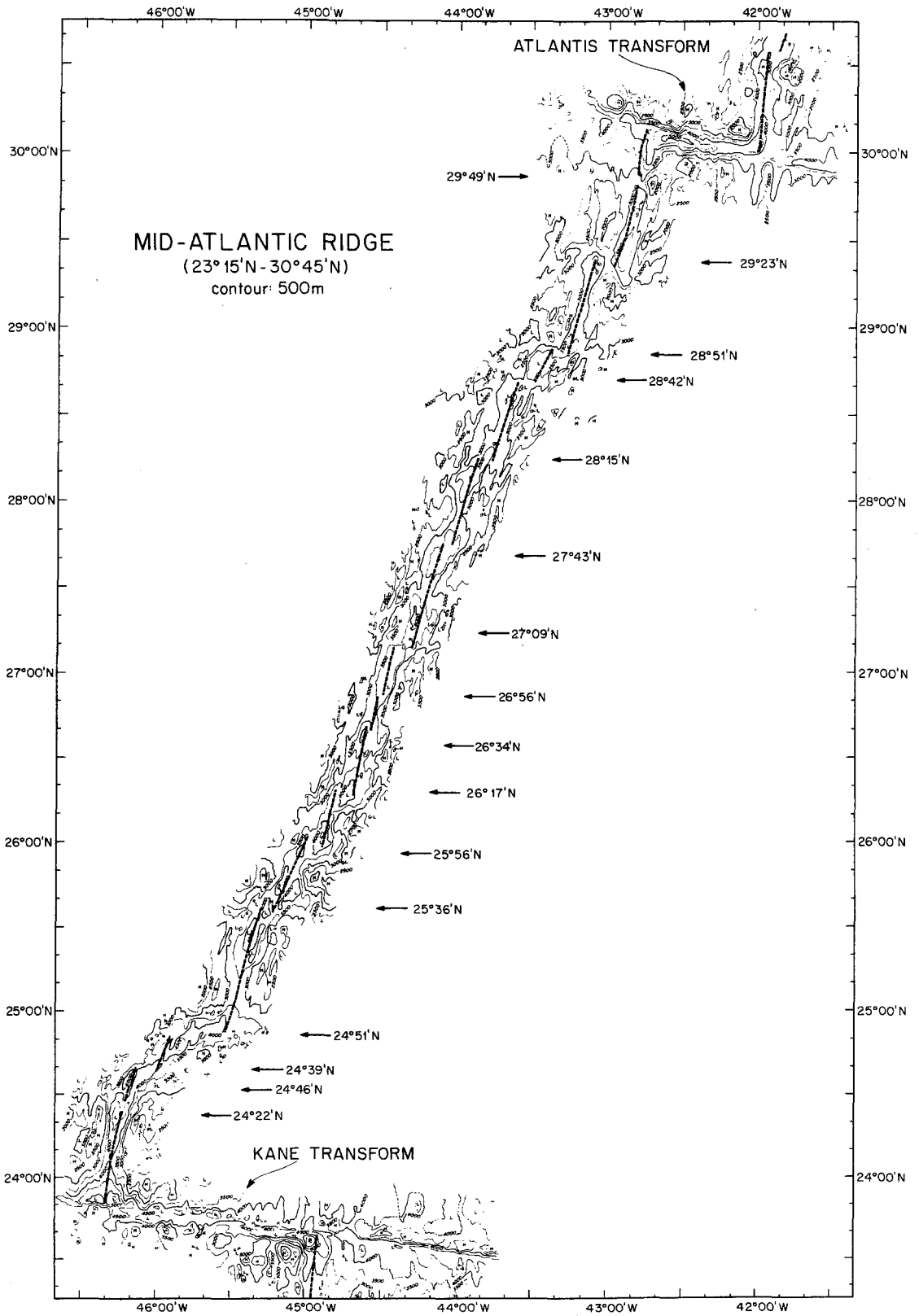

Fig. 1b. Bathymetry of the Mid-Atlantic Ridge between the Kane Transform (Pockalny *et al.*, 1988) and 30°40′ N (contour interval = 500 m). Dashed lines indicate major spreading segments.

inner valley floor. Terminal basins refer to depressions at the ends of each segment within which the NVZ terminates. Nodal basins describe those bathymetric lows found at the intersection of the spreading center with a transform or a large non-transform offset (e.g., Fox and Gallo, 1984).

We use the morphology of off-axis seafloor to study the temporal evolution of non-transform discontinuities. Because our own coverage is limited to 2-Ma-old lithosphere, we also use the widely-spaced (10–20 km), narrowbeam data of *Rona* (1976) between 24° and 27°N which extend out to 7-Ma-old crust. Finally we use the results of the inversion of the magnetic field over the spreading center to study the evolution of the discontinuities. Our coverage limits us to the Brunhes–Matuyama (B–M) boundary. The reader should keep in mind that the validity of the interpretation of surface magnetic data is restricted to wavelengths greater than ~3 km (Miller, 1977).

3. Segmentation of the Mid-Atlantic Ridge Between 24°00′ N and 30°40′ N

3.1. General characteristics

Analysis of Sea Beam bathymetry along the Mid-Atlantic Ridge between the Kane Fracture Zone and 30°40′N (full spreading rate = 23.6 mm a^{-1}; Argus *et al.*, 1989) reveals the scale and nature of the segmentation of this slow-spreading center (Figure 1b). Transform and non-transform discontinuities define spreading segments whose lengths vary from 10 to 85 km (Figures 1b, 2). A detailed description of the spreading segments and their boundaries is given in the appendix (Figures 3–11). Prior to our study, it was commonly assumed that transform faults offset the MAR with an average spacing of about 50 km (Macdonald, 1986). However, there are no transform offsets along the 800-km-long portion of the spreading center that we have studied except for the Atlantis Transform near 30° N. Instead, the spreading center is offset by non-transform discontinuities with morphologies quite different from that of transform faults (Fox and Gallo, 1986). At these discontinuities, the horizontal shear between the offset spreading segments is not accommodated along a sustained, narrow strike-slip zone. The morphology of these offsets is distinct from that of axial discontinuities at fast-spreading centers such as the EPR (e.g., Macdonald *et al.*, 1988), but it is similar to that of discontinuities along the MAR in the South Atlantic (e.g., Grindlay *et al.*, 1991). Non-transform discontinuities have offsets which range from ~0 to 30 km.

The segmented nature of the MAR is apparent in the along-axis variations of the depth of the spreading center. The axial depth profile of the MAR within our survey area exhibits intermediate-wavelength (10–100 km) variations with peak-to-trough relief ranging between 300 and 2200 m (Figure 2). Except for the 29°49′ N offset all spreading center discontinuities are located at local depth maxima. Transform offsets correspond to the largest depth anomalies (1000–2200 m), whereas non-transform discontinuities are associated with along-axis depth anomalies on the order of 300–900 m. The inner floor of the rift valley is shallowest near the middle of each segment and deepens toward the discontinuities. These depth variations are similar to those observed along the EPR (Macdonald *et al.*, 1984). They are superposed on the long-wavelength undulation in the depth of the rift valley between the Kane and the Atlantis Fracture Zones, and on the even-longer-wavelength decrease in the depth of the spreading center toward the Azores Triple Junction (LeDouaran and Francheteau, 1981).

3.2. Spreading center discontinuities

A hierarchy of spreading center discontinuities, based on their morphology and their spatial stability, has emerged from high-resolution studies of the mid-ocean ridge system (e.g., Macdonald *et al.*, 1988; Grindlay *et al.*, 1991). The present study provides new information on the nature of spreading center discontinuities along the MAR in the North Atlantic. Previously-recognized, short-offset discontinuities along the MAR in the North Atlantic fall within the spectrum of discontinuities observed between 24°00′ N and 30°40′ N (e.g., Detrick *et al.*, 1973; Searle and Laughton, 1977; Phillips and Fleming, 1977; Ramberg *et al.*, 1977; Choukroune *et al.*, 1978; Goud and Karson, 1985; Karson *et al.*, 1987; Kong *et al.*, 1988).

Transform Faults

Transform faults constitute the first-order segmentation of the MAR. They are associated with the largest spatial (>20–30 km) and age (>2–3 Ma)

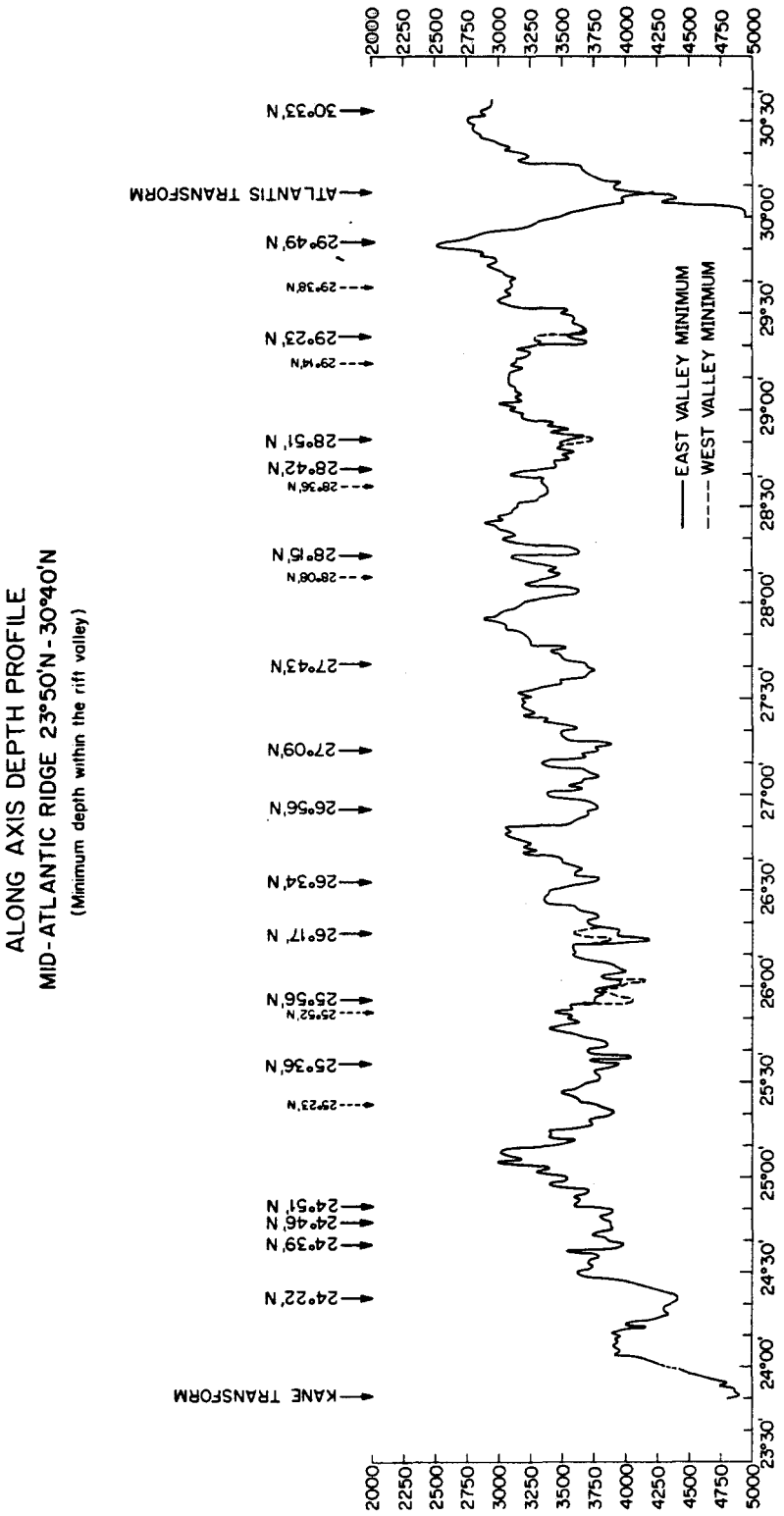

Fig. 2. Along-axis depth variations between the Kane Transform and 30°40′ N (minimum depth within the inner floor of the rift valley plotted at every minute of latitude). Spreading center discontinuities, which are located near along-axis depth maxima, bound the intermediate-wavelength undulations of the spreading center. Along-axis depth variations are on the order of 600 m for segments bounded by non-transform discontinuities and on the order of 800–1200 m for those bounded by the Kane or the Atlantis Transform. Small offset disruptions of the neovolcanic zone are marked by dashed lines.

offsets (Searle, 1986; Tamsett and Searle, 1988). They partition the MAR at intervals of 200–800 km by offsetting ridge segments along narrow, strike-slip fault zones (Fox and Gallo, 1986). Transforms are associated with large, along-axis depth anomalies (1000–2500 m), which are only partly explained by the contrast in thermal structure created by the juxtaposition of old lithosphere against the ridge axis (Parmentier and Forsyth, 1985). Transforms constitute boundaries which separate spreading segments for at least several Ma. Their off-axis traces follow portions of small circles that mark the past direction of relative plate motion, indicating that transforms do not migrate along axis. Slow-slipping transform faults are characterized by a broad, deep valley which contains a 1–5-km tectonized band created by the time-integrated motion of the transform fault zone (Fox and Gallo, 1984, 1986).

Non-Transform Discontinuities

Non-transform offsets are more numerous than transform faults along the MAR. They allow adjacent spreading segments with different tectonic styles, levels of magmatic activity, and extensional rates to coexist (Karson, 1990). Similar offsets are observed between segments of continental rifts where they are referred to as accommodation (Bosworth, 1985; Karson, 1990) or transfer zones (Gibbs, 1990; Morley *et al.*, 1990).

Second-order discontinuities consist of those non-transform offsets flanked by off-axis discordant zones that do not follow small circles about the pole of opening of the two plates (Macdonald *et al.*, 1988) (Figure 12). They correspond to spatial offsets of ~15–30 km, and to age offsets of 1–3 Ma. They are complex discontinuities that partition the spreading center at intervals of 10–100 km. At such discontinuities, horizontal shear between the offset ridge segments is not accommodated by a sustained, narrow, transform zone. The discontinuities are associated with minor changes ($<10°$) in the strike of the neovolcanic zone. Despite their small offsets, they correspond to along-axis depth anomalies of several hundred meters. The presence of off-axis traces on the flanks of second-order discontinuities suggests that they persist for several Ma. The orientations of these traces show that the discontinuities migrate along the spreading center (Johnson and Vogt, 1973; Rona, 1976; Rona and Gray, 1980; Schouten *et al.*, 1987; Tucholke and Schouten, 1988). Within our survey area, the 24°39′ N, 24°51′ N, 25°36′ N, 25°56′ N, 27°09′ N, 28°15′ N, 28°42′ N, 28°51′ N, and 29°23′ N offsets are second-order discontinuities (Figures 3a–9a).

Third-order discontinuities have characteristics similar to those of second-order offsets except that they are not associated with recognizable, off-axis traces (Figure 13) (Macdonald *et al.*, 1988; Grindlay *et al.*, 1991). They coincide with depth anomalies of a few hundred meters despite their small lateral offsets (<10 km). They may be associated with small reorientations ($<5°$) of the neovolcanic zone and abrupt steps in the rift valley walls. The absence of off-axis discordant zones indicates that third-order discontinuities are short-lived features, or that they may be newly-forming second-order discontinuities. Within our survey area, the 24°22′ N, 24°46′ N, 26°17′ N, 26°34′ N, 26°56′ N, 27°43′ N, 29°49′ N, and 30°33′ N offsets are third-order discontinuities (Figures 3a, 6a, 7a, 9a, 10a).

The morphology of second- and third-order discontinuities appears partially controlled by the distance between the offset spreading segments. Between the Kane and Atlantis Transforms, the largest of the non-transform discontinuities (24°51′ N Discontinuity, Figure 4a) is morphologically akin to transform faults. It is associated with features reminiscent of nodal basins. Features such as the 24°51′ N Discontinuity and FZ A in the FAMOUS area (Phillips and Fleming, 1977) may correspond to offset distances (20–30 km) transitional between transform and non-transform discontinuities. For smaller offset distances (15–25 km), but greater than the width of the rift valleys, the discontinuities are associated with offset rift segments separated by a fault-bounded high, possibly a fragment of the rift mountains flanking the spreading center (i.e. 29°23′ N, Figure 9a). When the offset becomes smaller than the width of the rift valleys, the discontinuities form intra-rift offsets. Intra-rift offsets are accommodated by extensional relay zones and/or linear volcanic constructions, parallel to sub-parallel to the spreading axis, which may result from extension in the intra-offset area.

Fourth-order discontinuities are minor offsets (<4 km) of the neovolcanic zone which do not disrupt the continuity of the rift valley. They constitute the smallest-scale segmentation that we

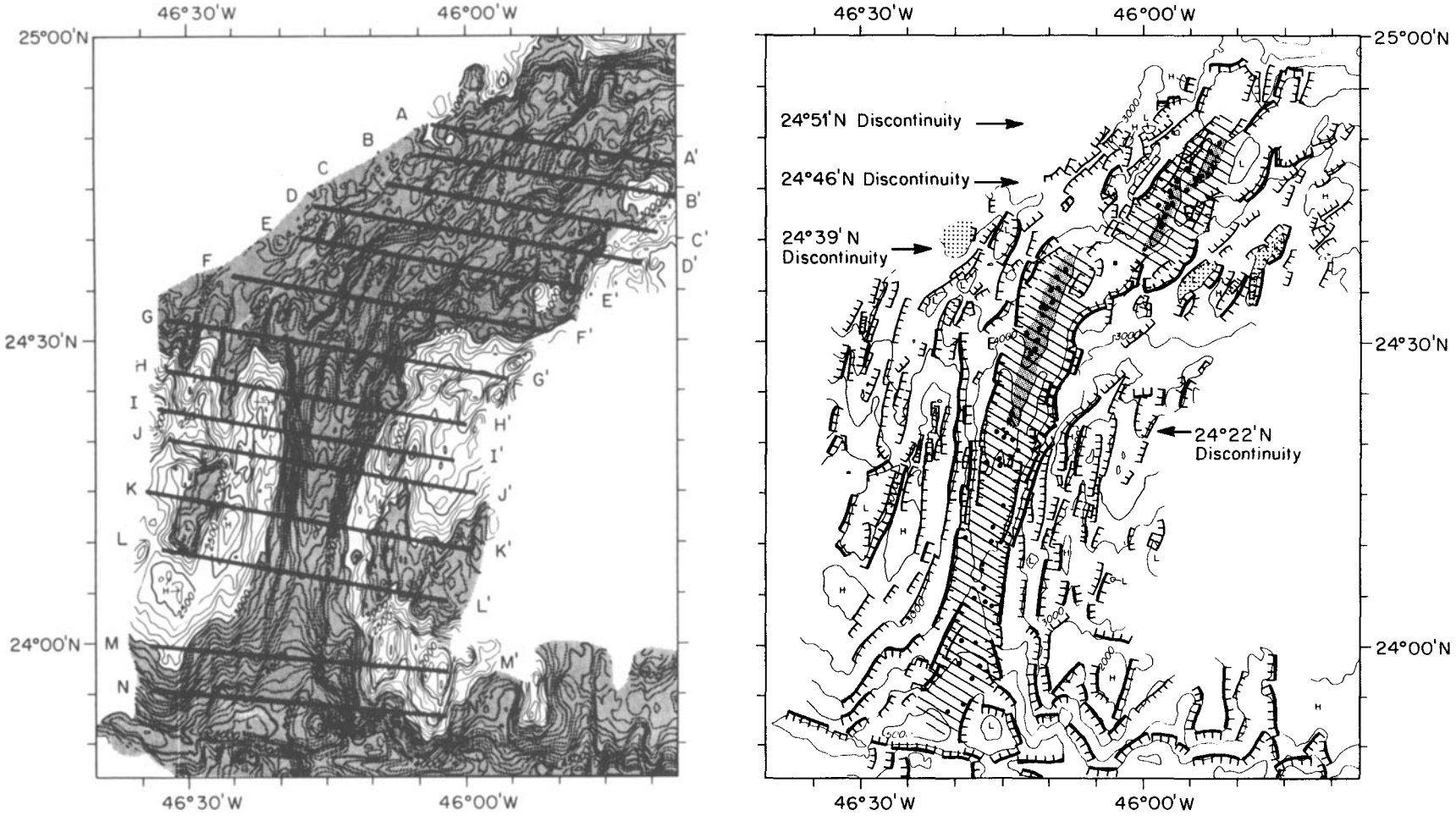

Fig. 3a. (left) Bathymetry of the Mid-Atlantic Ridge between the Kane Transform and latitude 25°00′ N. Contour interval is 100 m. Areas deeper than 3000 m are shaded. The bathymetric map is only meant to give the reader a large-scale view of the spreading center and is not intended for detailed analysis of small-scale, morphotectonic units. The reader is referred to the 30 inches/degree maps of Purdy *et al.* (1990) for a detailed view of the bathymetric data. (right) Interpreted structural geomorphology. Contour interval is 500 m. Hachures indicate the dip direction of the faults. See Figure 4a for legend.

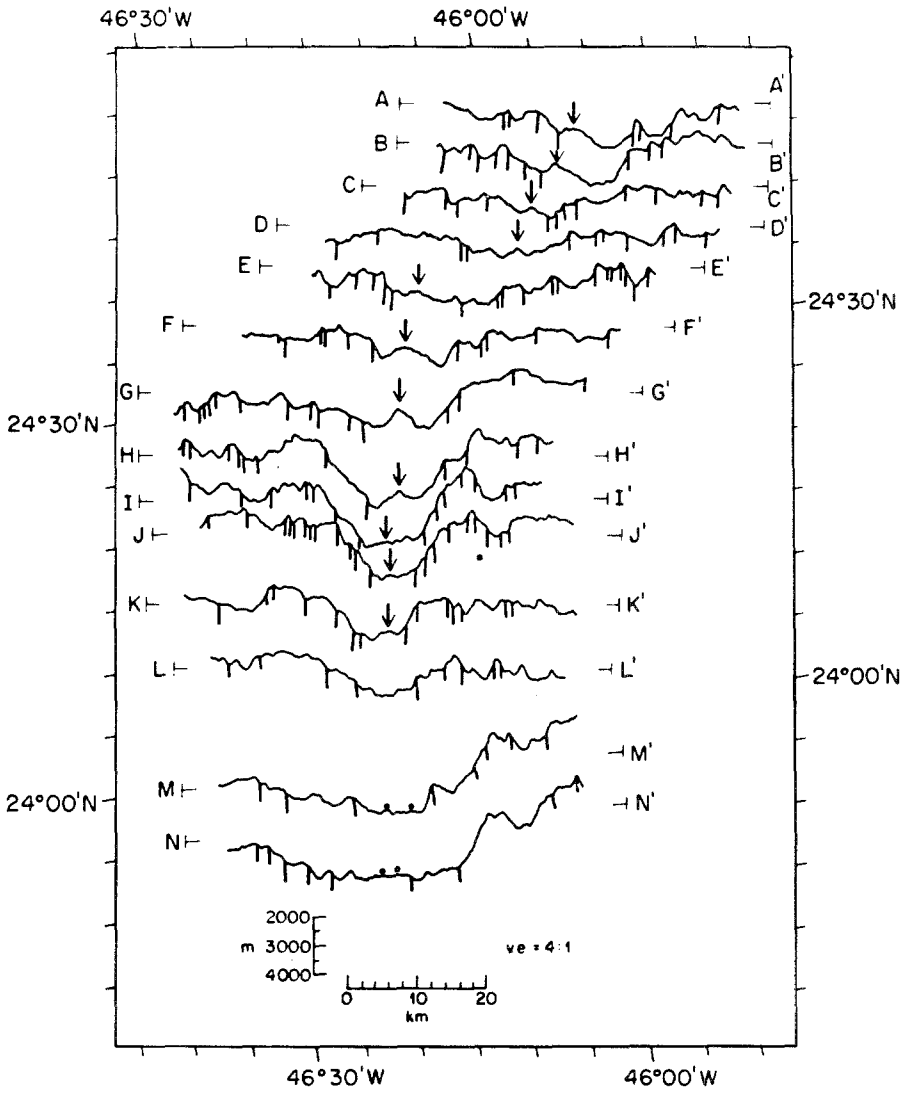

Fig. 3b. Bathymetric profiles across the rift valley of the Mid-Atlantic Ridge between the Kane Transform and latitude 25°00′ N. Profiles are projected along a 100° azimuth except for the two southernmost ones which are projected along a 095° azimuth. The location of faults are inferred from Sea Beam data. Fault dips are unconstrained. The reference level of each profile is 3000 m. Vertical exaggeration is 4:1. Vertical arrows indicate the location of the neovolcanic zone, filled circles volcanoes within the inner floor. See Figure 3a for location of profiles.

presently recognize. They are associated with small (<200 m) along-axis depth anomalies which bound short-wavelength undulations of the spreading center (Figure 2). When the neovolcanic zone is not located on top of a continuous ridge, fourth-order discontinuities correspond to gaps between the individual volcanoes or strings of volcanoes that compose the neovolcanic zone (Figure 13). When the neovolcanic zone lies on top of a ridge, fourth-order discontinuities correspond to offsets in these ridges and to small changes in their orientation (<10°). These offsets often consist of two overlapping ridges separated by an elongate depression (Figure 11). One or both ridges may curve toward the other one. Such a morphology is similar to that of overlapping spreading centers along the EPR (Macdonald *et al.*, 1984). It may result from the propagation and interaction of fracture systems associated with the emplacement of the two offset neovolcanic ridges (e.g., Pollard and Aydin, 1984; Sempéré and Macdonald, 1986). Within our survey area, we interpret the 25°23′ N, 25°52′ N, 28°08′ N, 28°36′ N, 29°14′ N, and 29°38′ N offsets as minor discontinuities of the neovolcanic ridge (Figure 11).

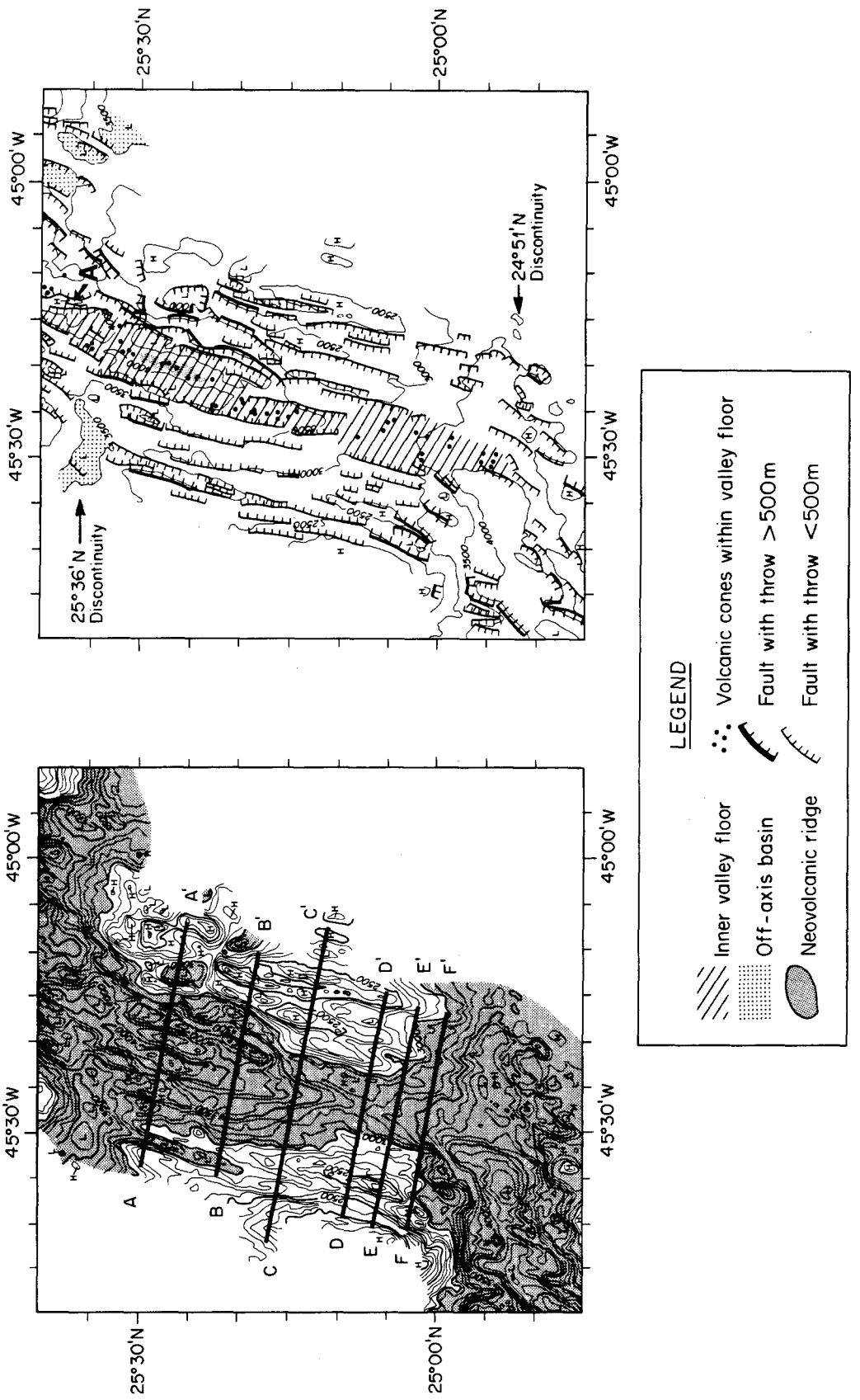

Fig. 4a. Bathymetry and structural geomorphology of the 24°51′–25°36′ N segment.

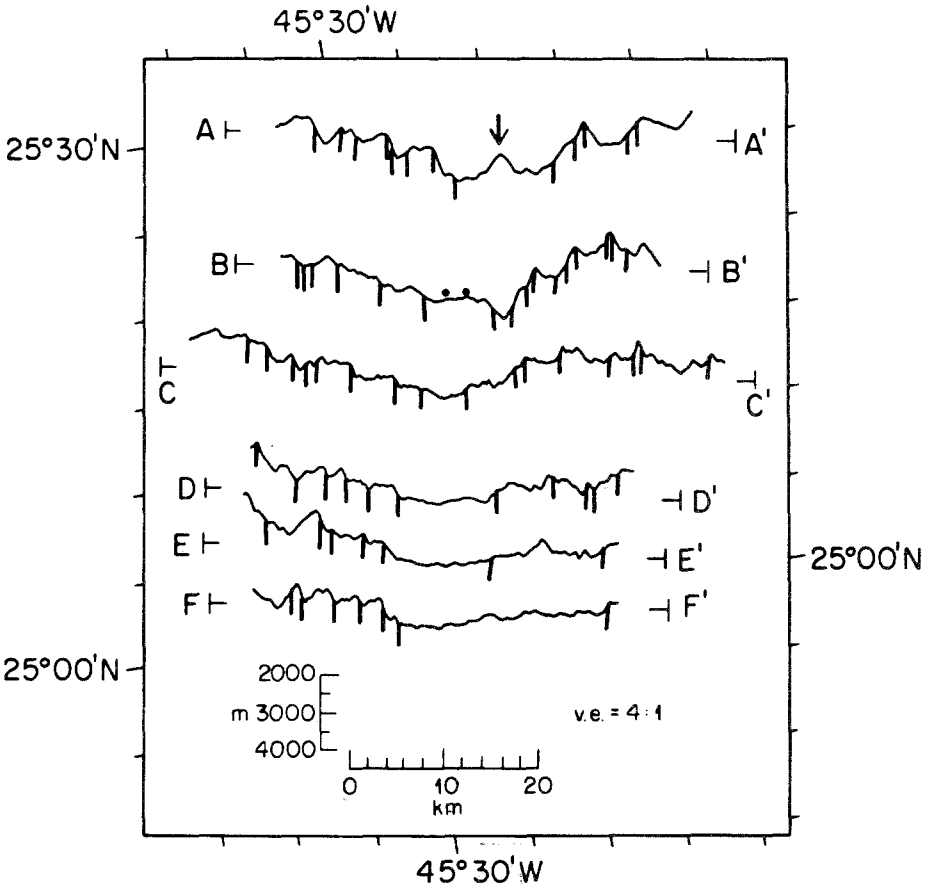

Fig. 4b. Bathymetric profiles across the 24°51′–25°36′ N segment. See Figure 4a for location of profiles.

3.3. Migration of non-transform discontinuities

Second-order discontinuities are flanked with basins, which have morphologies and sizes akin to those of terminal lows found near the ends of each segment, or with valleys slightly oblique to the spreading direction. The basins may be the fossil equivalents of the on-axis terminal lows. They integrate spatially to form discordant zones which interrupt the continuity of the rift mountain terrain, and which offset geomagnetic reversal boundaries on the flanks of the discontinuities (e.g., Brown *et al.*, 1990). These traces are not well-defined in our coverage due to its limited off-axis extent. However, between 24° N and 27° N, the location and orientation of the off-axis traces inferred from our study coincide with those based on narrow-beam coverage out to ~7-Ma-old lithosphere (Rona and Gray, 1980). We suggest that these lineaments mark the traces of second-order discontinuities in off-axis seafloor. As new lithosphere is accreted at the axis and as seafloor is transported from the inner floor outside the rift valley, terminal lows are incorporated in the rift mountains and integrate laterally to form off-axis, discordant traces (Figure 14).

The presence of off-axis traces indicates that second-order discontinuities have persisted with time. These traces differ from fracture zones in that they do not follow small circles about the pole of opening of the two plates, indicating that the discontinuities are not stable with respect to the plate boundary. Between the Kane and Atlantis Transforms, off-axis discordant zones appear to form V-shaped lineaments pointing toward north, as observed in the TAG and MARK areas (Figure 15) (Rona *et al.*, 1976; Rona and Gray, 1980; Tucholke and Schouten, 1988; Kong *et al.*, 1988). Following Johnson and Vogt (1973) and Schouten *et al.* (1987), we interpret the V-shaped, discordant zones as reflecting the northward migration of non-transform offsets with respect to the spreading center over the last

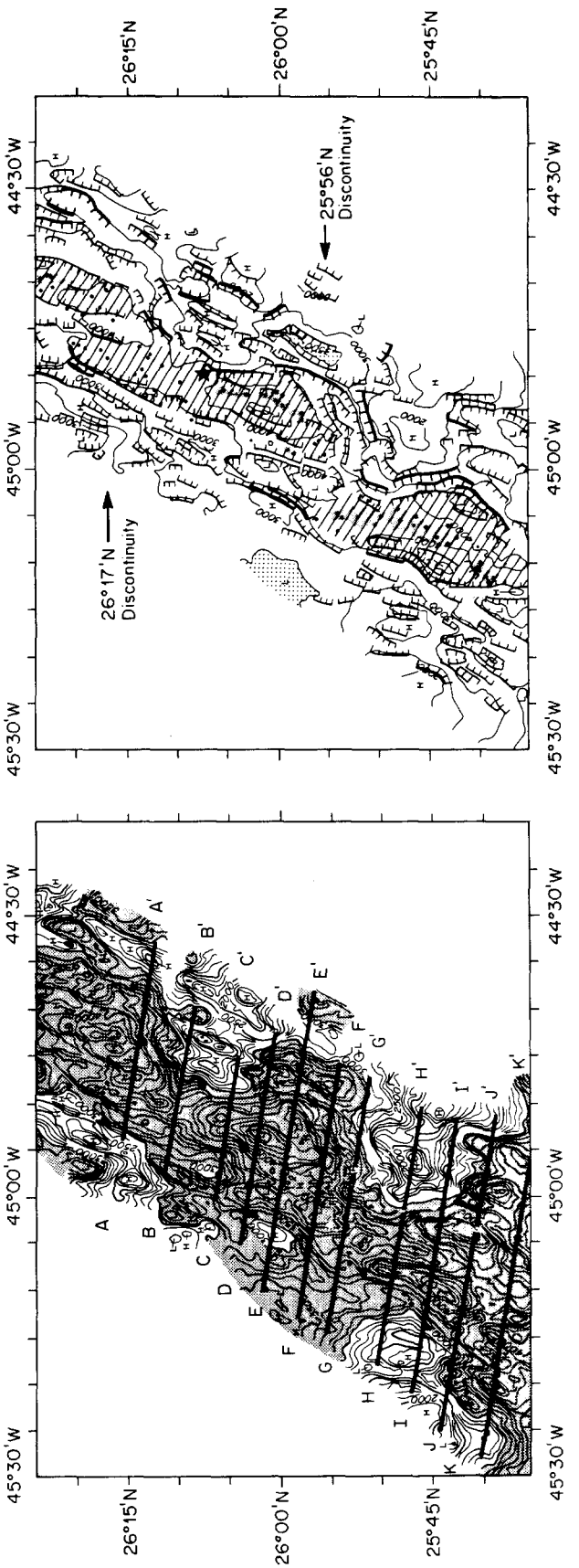

Fig. 5a. Bathymetry and structural geomorphology of the 25°36′–25°56′ N and 25°56′–26°17′ N segments. The TAG hydrothermal field area is represented by a star. See Figure 4a for legend.

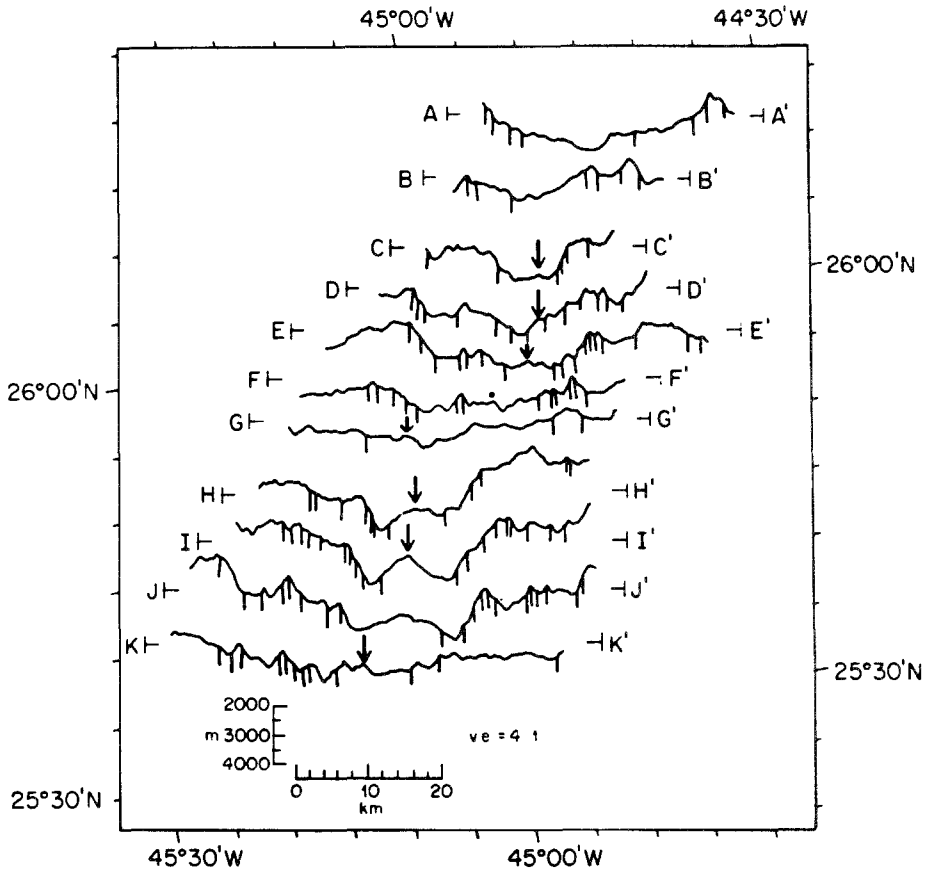

Fig. 5b. Bathymetric profiles across the 25°36′–25°56′ N and 25°56′–26°17′ N segments. See Figure 5a for location of profiles.

2 Ma. The validity of this result is limited due to the fact that the discordant traces are defined by only 1–4 basins within our coverage because of its short off-axis extent. A more recent Sea Beam survey indicates that, between 28° N and 29° N, the direction of migration of discontinuities agrees with our interpretation for the last 3 Ma, but that, between 3 and 10 Ma, migration was toward the south (Patriat *et al.*, 1990; Brown *et al.*, 1990).

Because the offsets have migrated 'uphill', over the last 2 Ma, with respect to the long-wavelength depth variations of the MAR, we conclude that regional topographic gradients do not control the migration direction of non-transform discontinuities. The orientation of off-axis discordant zones may instead reflect the southward migration of the spreading center with respect to an asthenospheric reference frame, as proposed by Schouten *et al.* (1987). However, off-axis coverage between 28° N and 29° N shows that the migration direction of some of the offsets changed from southward to northward ~3 Ma ago (Patriat *et al.*, 1990; Brown *et al.*, 1990), indicating that local processes may be more important in controlling the migration of non-transform discontinuities.

3.4. Segmentation of the Mid-Atlantic Ridge: Model and Causes

Although the pattern of mantle upwelling beneath mid-ocean ridges in general, and the MAR in particular, is largely unknown, the different wavelengths of along-axis depth variations (e.g., LeDouaran and Francheteau, 1981) suggest different length scales for the segmentation of the MAR and the upwelling of asthenospheric material beneath it (Figure 16). On a global scale, the very long-wavelength variations in the depth of the MAR (1000–5000 km) may be strongly influenced by upwelling from the deep mantle, possibly related to hot spots, and may correspond to the deepest-level segmentation. In particular, the long-wavelength gradient in the depth of the MAR in the central North Atlantic is due to the

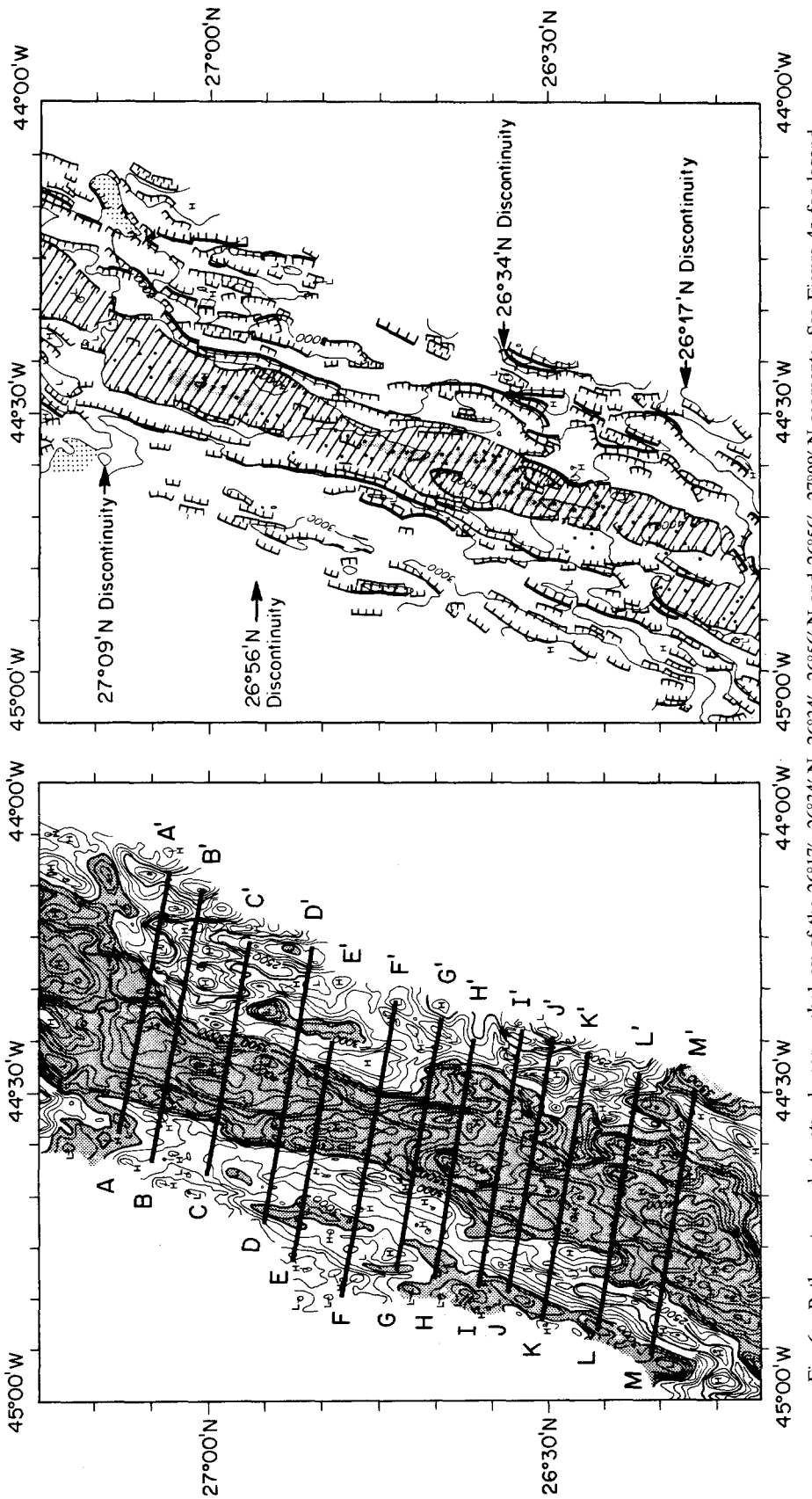

Fig. 6a. Bathymetry and structural geomorphology of the 26°17′–26°34′ N, 26°34′–26°56′ N and 26°56′–27°09′ N segments. See Figure 4a for legend.

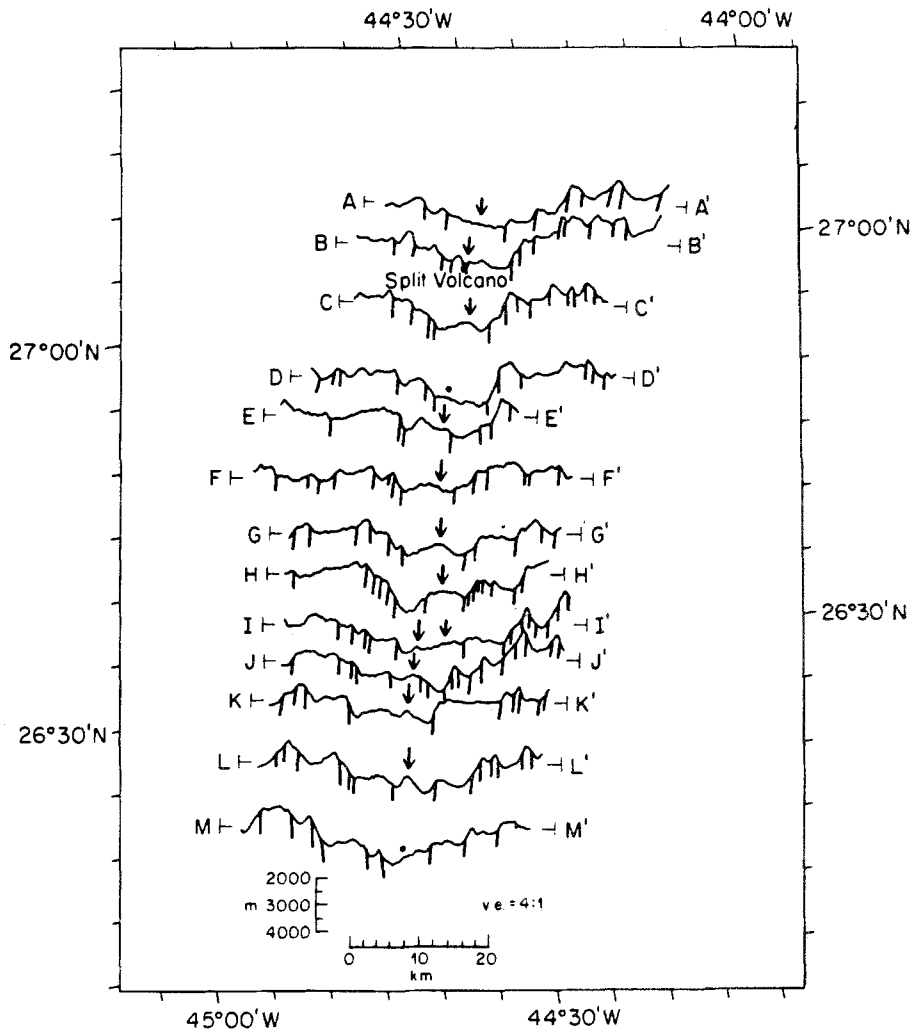

Fig. 6b. Bathymetric profiles across the 26°17′–26°34′ N, 26°34′–27°09′ N and 26°56′–27°09′ N segments. See Figure 6a for location of profiles.

Azores hot spot (LeDouaran and Francheteau, 1981). This very-long wavelength segmentation may correspond to a geochemical and isotopic segmentation. The tectonic boundaries of the isotopic segmentation may coincide with large transforms, such as the Charlie-Gibbs and Kane F. Z.'s, as evidenced by discontinuities in isotopic ratios at these localities (Schilling, 1986).

At a scale of 200–1000 km, the undulation of the depth of the MAR may reflect the long-wavelength upwelling of asthenospheric material between two transform faults. The three-dimensional flow structure of the upwelling asthenosphere may lead to another scale of segmentation by generating magmatic upwelling events which feed distinct spreading segments (e.g., Whitehead *et al.*, 1984; Crane, 1985; Schouten *et al.*, 1985; Dick, 1989; Rabinowicz *et al.*, 1990; Parmentier and Phipps Morgan, 1990). The surficial expression of this smaller-length-scale segmentation (10–100 km) corresponds to non-transform discontinuities. The migration and youth of some of the offsets indicate that the processes which cause the segmentation of the MAR are not spatially stable with respect to the spreading center and not continuous in time. Magmatic upwelling may be enhanced near the middle of each segment where the spreading center is shallowest (Figure 17). The lesser magma supply at the ends of segments is evidenced by the deepening of the spreading center toward the discontinuities. The emplacement of isolated volcanoes or volcanic ridges along the neovolcanic zone may be considered the surficial expression of a fine-

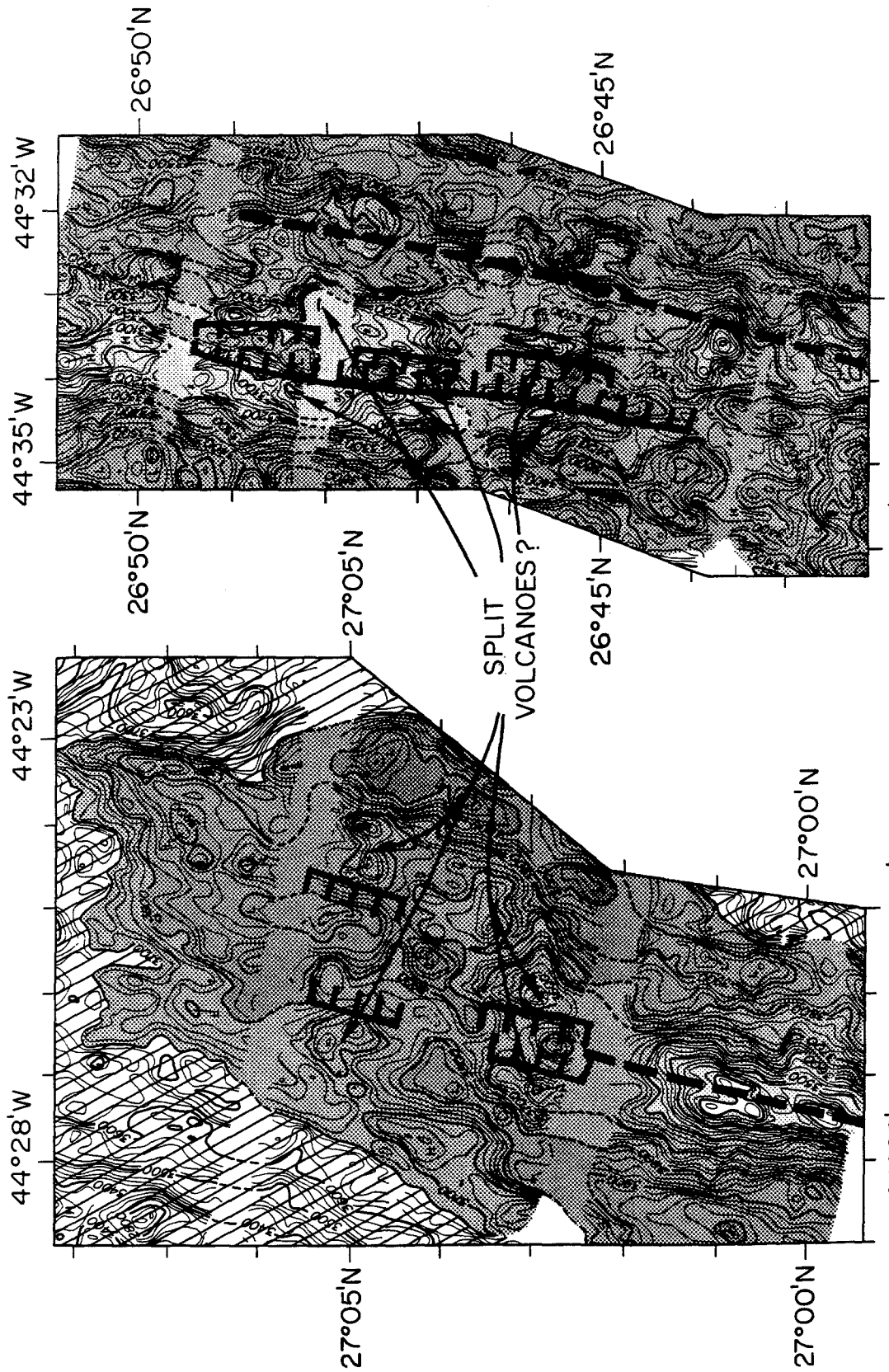

Fig. 6c. Split volcanoes within the inner floor of the Mid-Atlantic Ridge. The stippled pattern marks the inner valley walls. Faults bounding the split volcanic edifices are inferred from Sea Beam data. Shading interval is 200 m. The NVZ is shown by a dashed line.

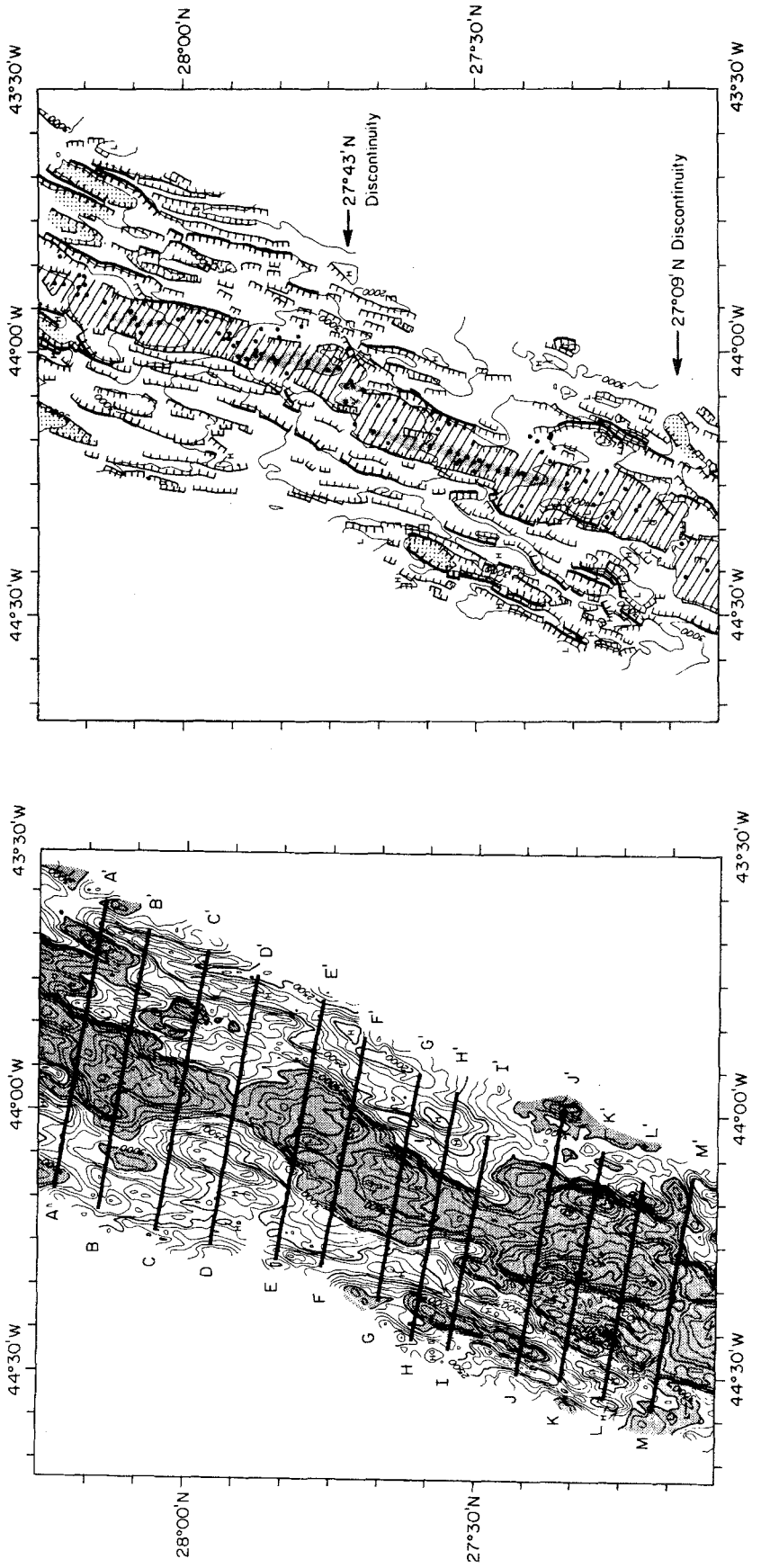

Fig. 7a. Bathymetry of the 27°09′–27°43′ N and 27°43′–28°15′ N segments.

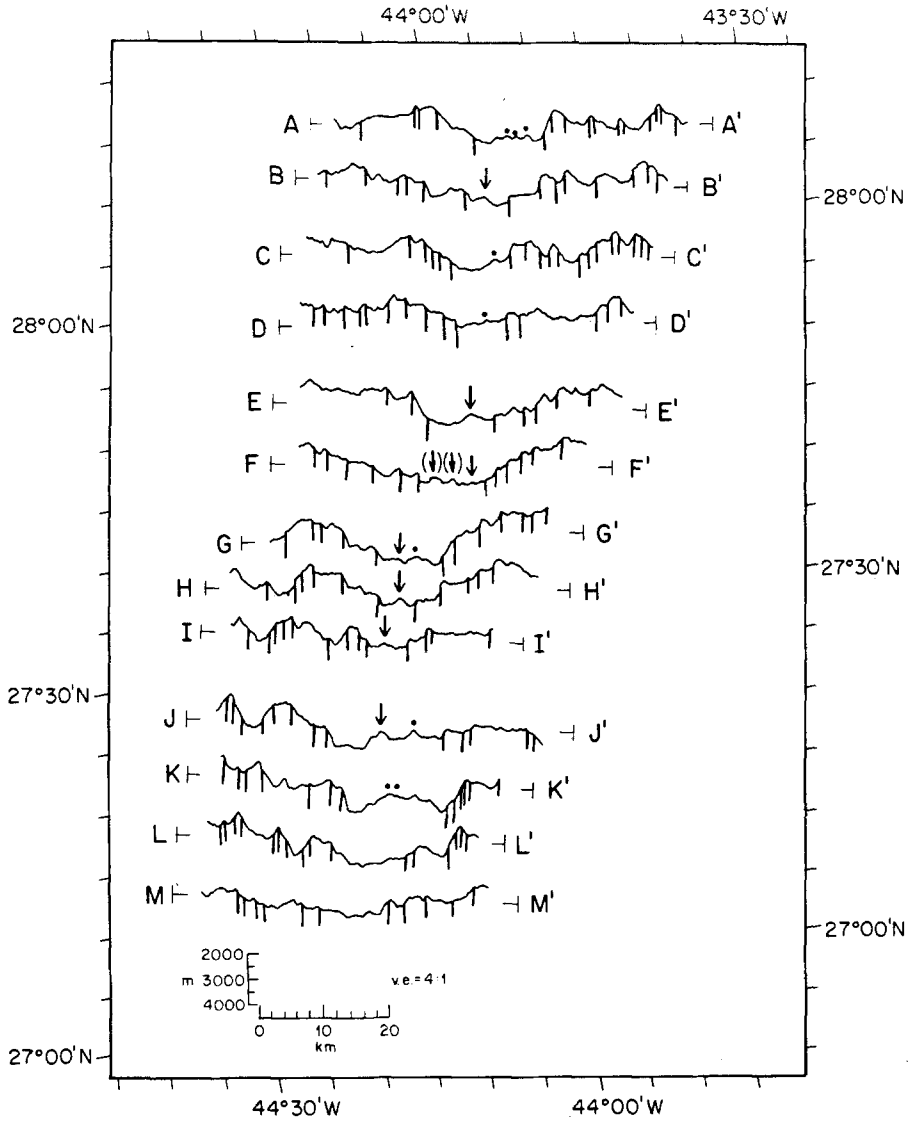

Fig. 7b. Structural geomorphology of the 27°09′–27°43′ N and 27°43′–28°15′ N segments. See Figure 4a for legend.

scale, volcanic segmentation. Small-offset disruptions of the neovolcanic zone correspond to the smallest discontinuities that we can presently resolve. If distinct sources in the upper mantle feed individual segments along the spreading center, the volcano-tectonic segmentation of the MAR will be associated with a geochemical segmentation which reflects differences in mantle sources feeding individual segments (e.g., Langmuir *et al.*, 1986). Due to inadequate sampling density, this can neither be confirmed nor dismissed for the MAR at this time (e.g., Melson and O'Hearn, 1986).

Mid-ocean ridges may have abrupt lateral offsets because spreading segments tend to remain orthogonal to the instantaneous direction of relative plate motion, whereas the spreading center as a whole does not (Lonsdale, 1989b). The obliquity between the overall trend of a mid-ocean ridge and the direction of plate separation is most commonly caused by a change in relative plate motion. Axial discontinuities can form, vary in size, or change in nature in response to changes in relative plate motion (Tucholke and Schouten, 1989; Lonsdale, 1989b; Grindlay *et al.*, 1991). The average trend of the neovolcanic zone within our survey area (013° ± 5°, excluding the 28°42′–28°51′ N segment) is perpendicular to the spreading direction (102°, Argus *et al.*, 1989), but is 13° oblique to the overall trend of the

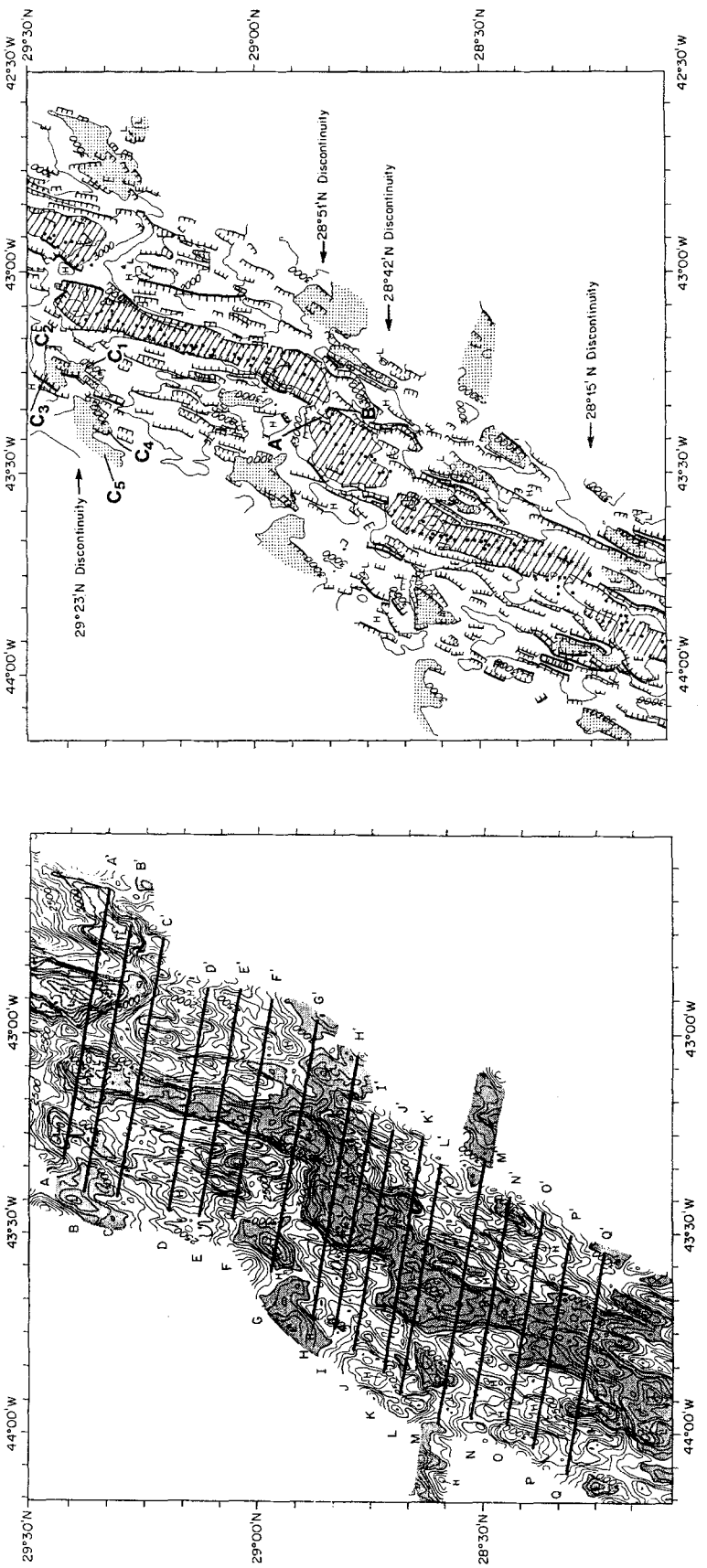

Fig. 8a. Bathymetry of the 28°15′–28°42′ N, 28°42′–28°51′ N and 28°51′–29°23′ N segments.

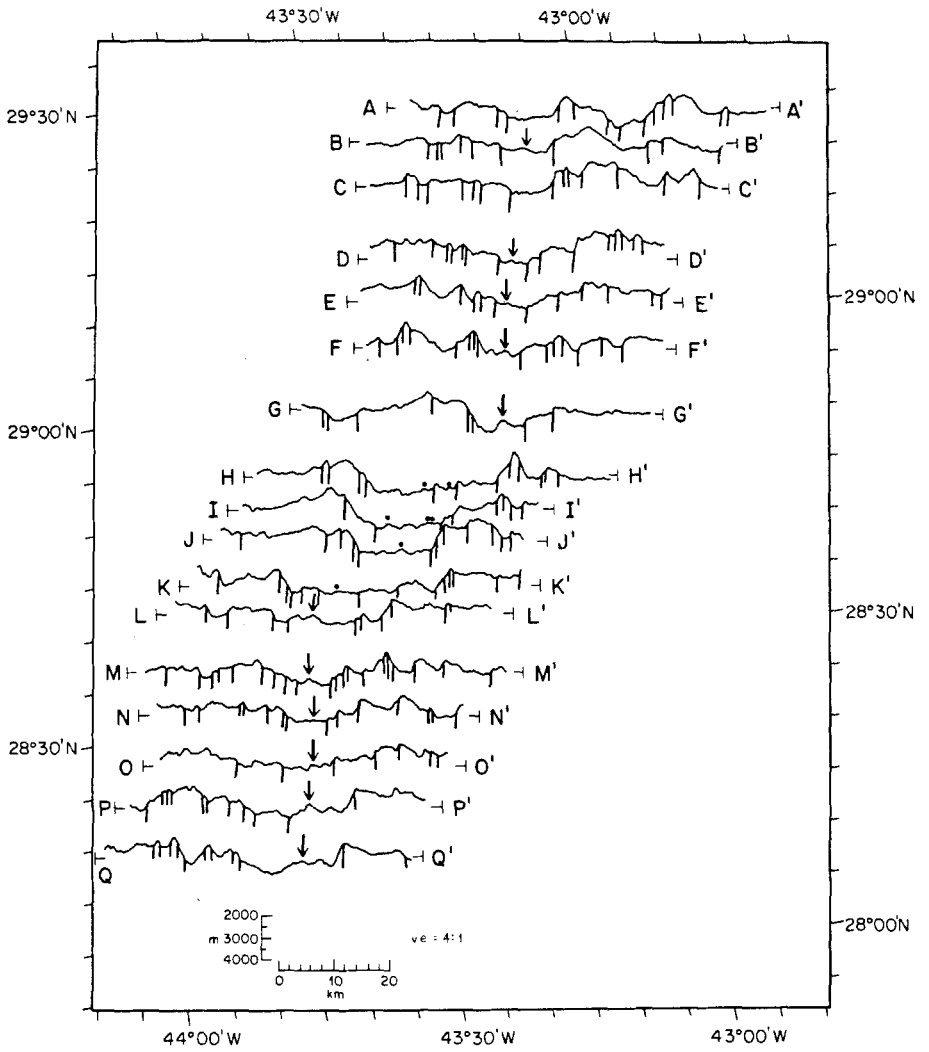

Fig. 8b. Structural geomorphology of the 28°15′–28°42′ N, 28°42′–28°51′ N and 28°51′–29°23′ N segments. See Figure 4a for legend.

MAR between the Kane and Atlantis Transforms (026°). All discontinuities between 24° N and 31° N with offsets greater than 5 km are right-stepping. This sense of offset is in agreement with the obliquity of the plate boundary with respect to the spreading direction because right-stepping discontinuities are necessary to accommodate a 100° spreading direction along a spreading center striking 026°. If the hypothesis of Lonsdale (1989b) is correct, the right-stepping pattern observed between the Kane and Atlantis Transforms is evidence for a recent, counterclockwise change in the direction of relative plate motion of ~13°. However, the most recent, large-scale adjustment to relative plate motion near our survey area is a 10° counterclockwise rotation that occurred between 22 Ma and the present, and more recent changes have been much smaller (Tucholke and Schouten, 1989).

4. Segmentation and Along-Axis Morphotectonic Variations

4.1. Inter-segment, volcano-tectonic variability

The spectrum of rift valley morphology observed between the Kane and Atlantis Transforms ranges from a narrow, deep, hourglass valley to a wide valley bounded by low-relief rift mountains. Within this broad spectrum, the distribution of rift valley morphologies falls into two primary groups.

Group I includes those segments characterized by a narrow and deep rift valley (Figure 18). These

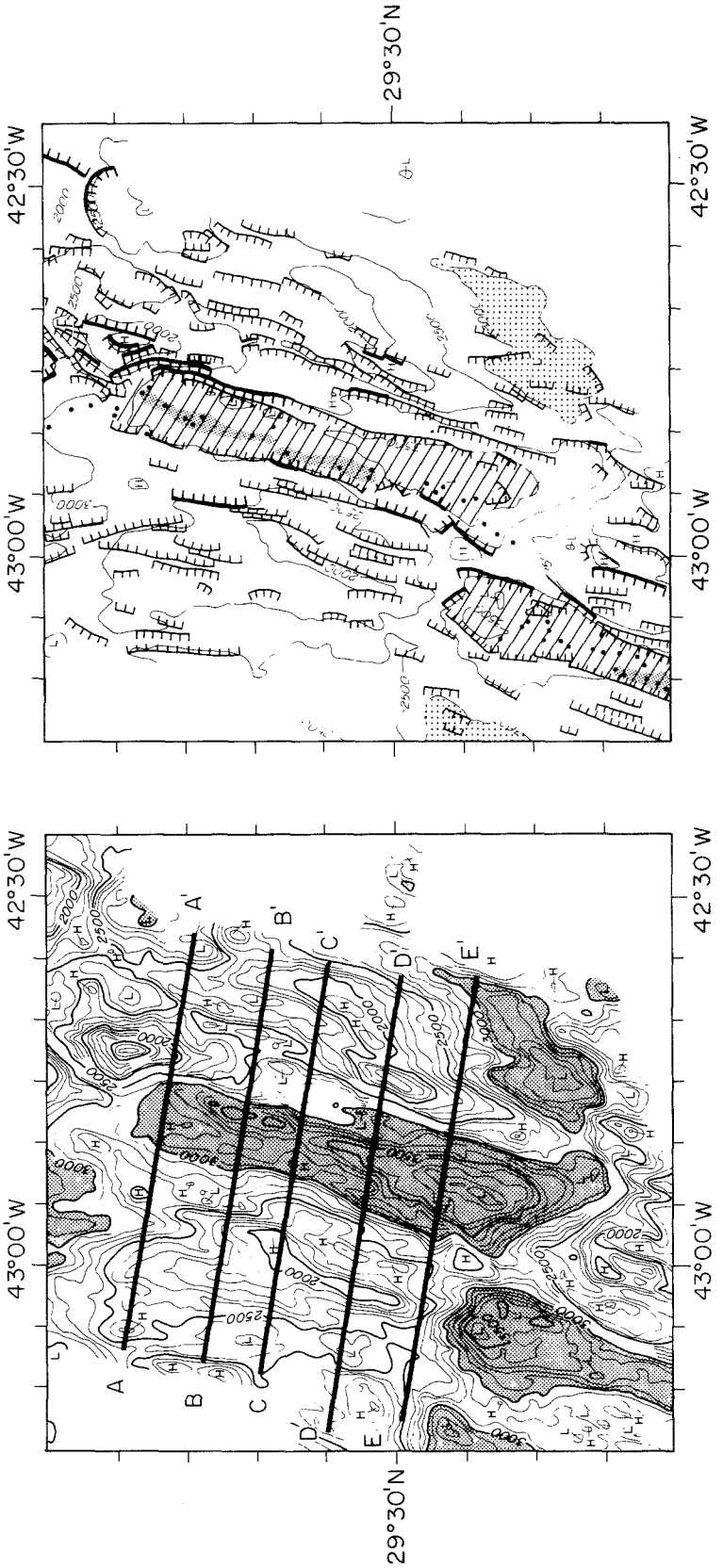

Fig. 9a. Bathymetry and structural geomorphology of the 29°23′–29°49′ N segment. See Figure 4a for legend.

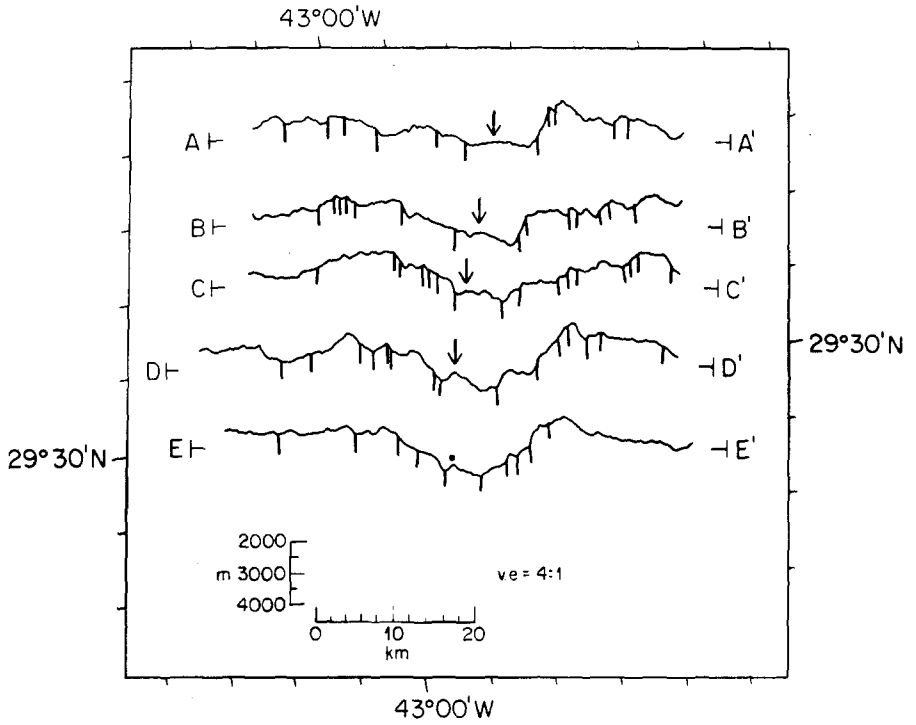

Fig. 9b. Bathymetric profiles across the 29°23′–29°49′ N segment. See Figure 9a for location of profiles.

segments have a V-shaped cross-section (e.g., profile J–J′ in Figure 3a) and a distinctive hourglass morphology in plan view. The waist of the hourglass occurs near the segment mid-point and coincides with the shallowest depth of the inner floor (~3000 m). The rift mountains consist of axis-parallel ridges and troughs which define a lineated fabric whose along-axis continuity is only interrupted by the off-axis traces of some of the non-transform discontinuities. Group I segments are found, for the most part, between 27°43′ N and 29°49′ N – the long-wavelength bathymetric high between the Kane and Atlantis Transforms. They appear to be associated with circular, mantle Bouguer anomalies centered over the segment mid-point which may be indicative of focused mantle upwelling and/or along-axis crustal thickness variations (Lin *et al.*, 1990). We classify the 25°36′–25°56′ N, 27°43′–28°15′ N, 28°15′–28°42′ N, 28°42′–28°51′ N, 28°51′–29°23′ N, 29°23′ N–29°49′ N and the Atlantis-30°33′ N segments as belonging to Group I. This classification is based on gravity data between 27°50′ N and 30°40′ N (Lin *et al.*, 1990) and 25°15′–26°45′ N (Zervas *et al.*, 1990). Although the 25°36′–25°56′ N segment is located away from the long-wavelength depth anomaly high, it appears to belong to Group I because of its association with a subcircular gravity low (Zervas *et al.*, 1990). Other segments within our coverage cannot be classified according to this scheme due to lack of gravity information. Based on morphology only, we suggest that the Kane-24°22′ N, 24°51′–25°36′ N segments and the Narrowgate rift (FAMOUS area) (Luyendyk and Macdonald, 1977; Macdonald and Luyendyk, 1977; Ballard and van Andel, 1977; Crane and Ballard, 1981) also belong to Group I.

Group II segments are associated with a wide inner valley, a U-shaped cross-section (e.g., profile F–F′ in Figure 3a) and a deep inner floor (Figure 18). The shallowest depth within the inner floor of these segments is ~3500 m, 500 m deeper than for Group I. Small, isolated basins often interrupt the continuity of rift mountain terrain. Group II segments are predominantly located between 24°30′–24°51′ N and 25°36′–27°43′ N, in the deepest part of the long-wavelength, along-axis depth profile between the Kane and Atlantis Transforms (Figure 2). Based on gravity data between 25°15′ N and 26°45′ N (Zervas *et al.*, 1990), these segments are not associated with circular, mantle Bouguer anomalies.

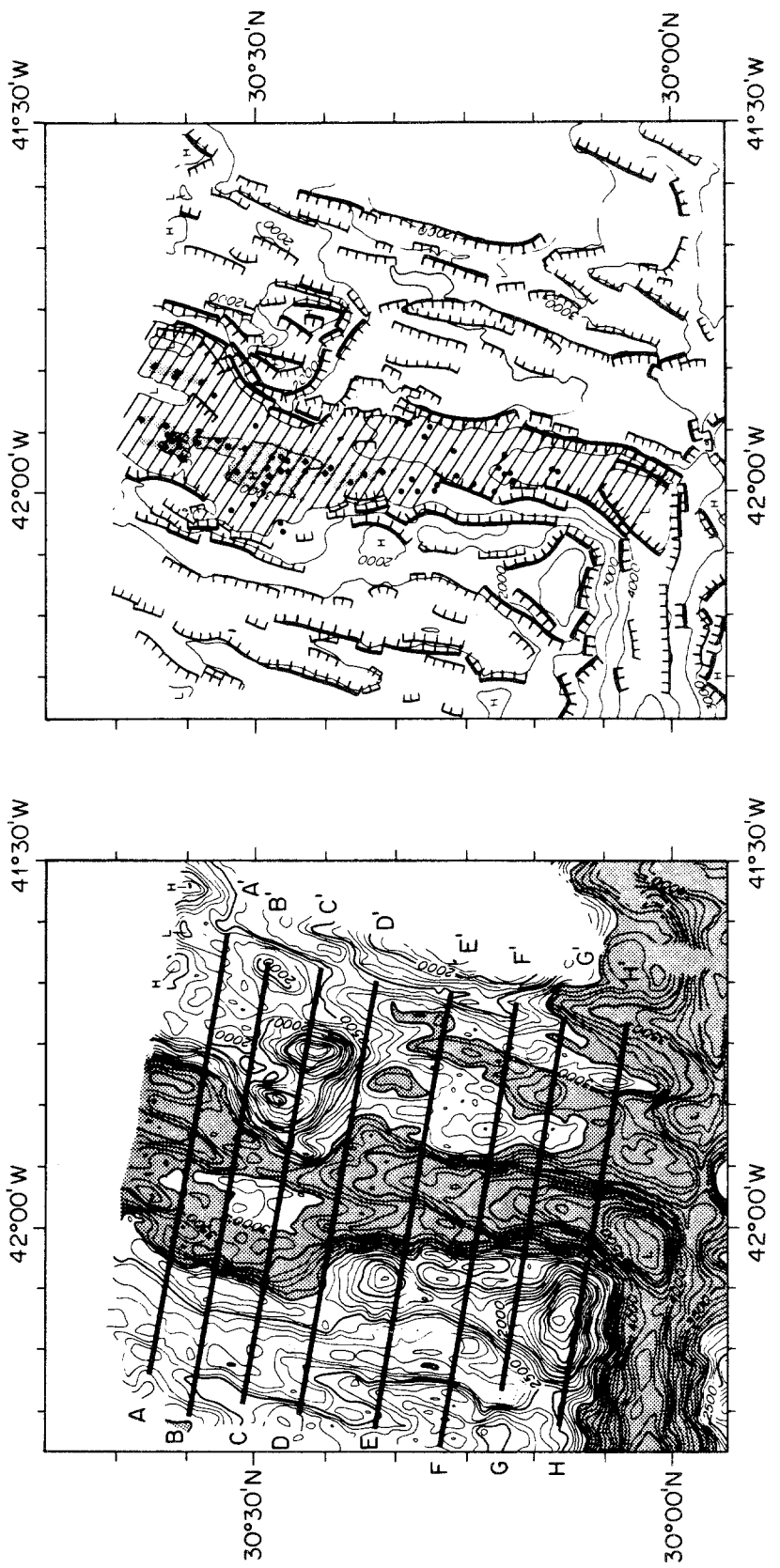

Fig. 10a. Bathymetry and structural geomorphology of the Atlantis-30°33′ N segment. See Figure 4a for legend.

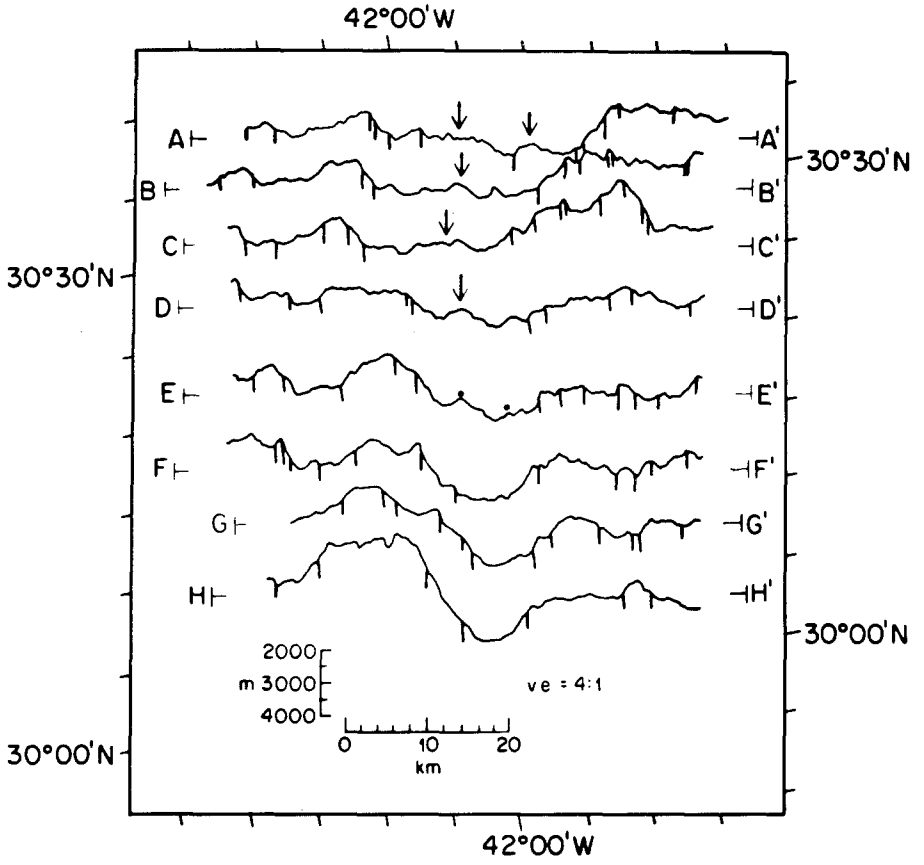

Fig. 10b. Bathymetric profiles across the Atlantis-30°33′ N segment. See Figure 10a for location of profiles.

Thus, mantle upwelling and/or crustal structure beneath Group II segments may be different than beneath Group I segments. We classify the 25°56′–26°17′ N and 26°17′–26°34′ N segments as belonging to Group II based on the gravity analysis of Zervas *et al.* (1990). The absence of a distinctive pattern of circular anomalies indicates that the northern segment of the MARK area belongs to Group II (Morris and Detrick, 1991).

Previous attempts to classify the morphology of the MAR have yielded two families of segments: one characterized by V-shaped rift valleys (a property of Group I segments), the other by U-shaped valleys (a property of Group II segments). This previous classification has been interpreted in terms of a cyclic, evolutionary model of the MAR in which volcanically- and tectonically-dominated phases alternate in time (e.g., Ballard and van Andel, 1977; Ramberg and van Andel, 1977; Crane and Ballard, 1981; Eberhard *et al.*, 1989). Such a cyclic model does not take into account the position within a segment of the portion of the spreading center considered. Our study shows large, along-axis variations in the volcano-tectonic characteristics of the spreading center within and between segments, and indicates that the three-dimensional nature of crustal accretion must be taken into account in models of the evolution of the plate boundary. We propose that the first-order morphology of spreading segments may be controlled by the pattern of upwelling mantle flow beneath the segments, and associated crustal structure variations. Our classification of segment morphology postulates major differences between spreading segments which are related to the structure of the crust and shallow mantle beneath them. Narrow, hourglass segments and V-shaped cross-sections (Group I) are associated with circular mantle Bouguer anomalies (i.e., focused mantle upwelling?), more robust volcanism, and less widespread tectonic activity. These segments may be experiencing a phase of voluminous, sustained and focused magma upwelling and melt production, and thus may be dominated by

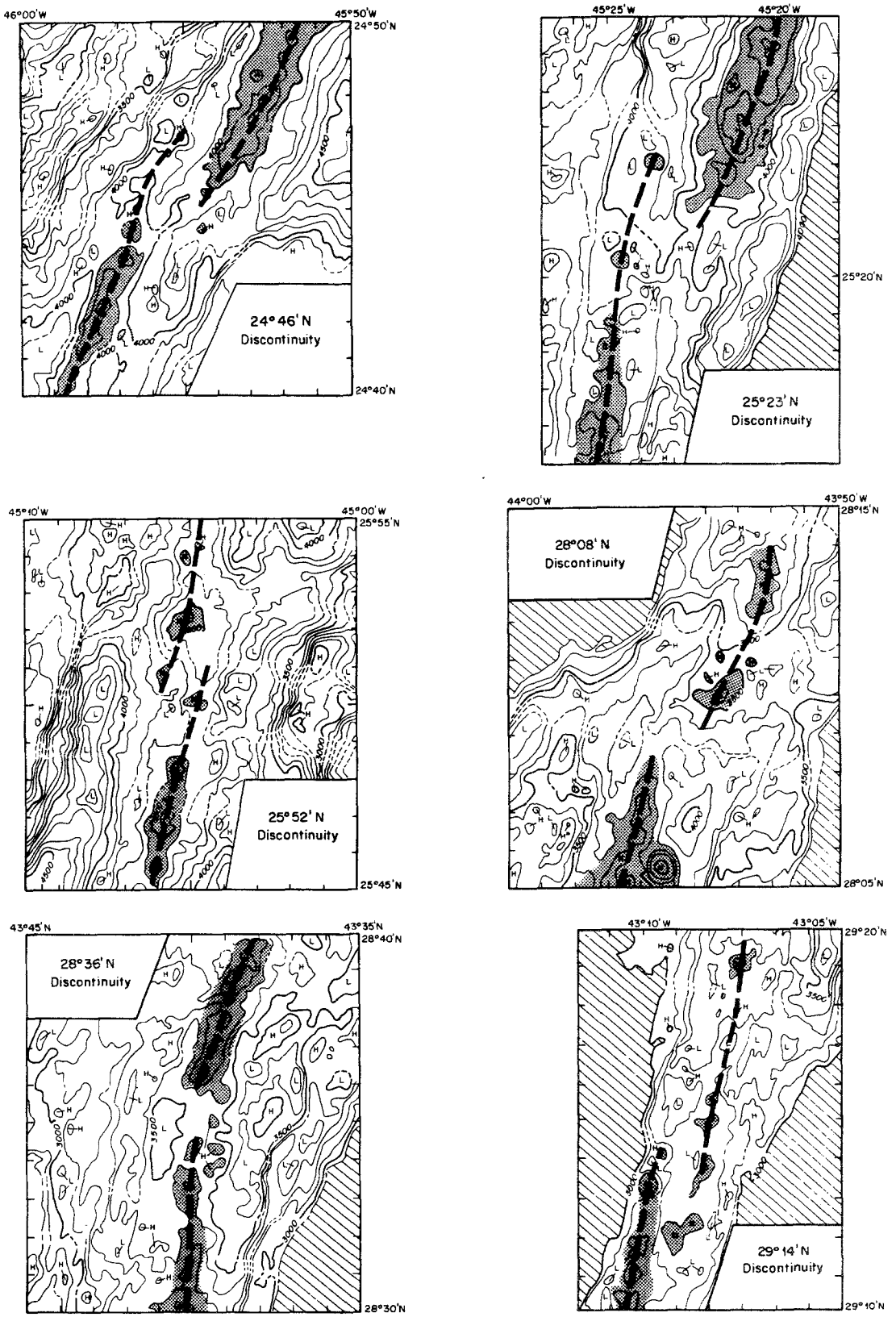

Fig. 11. Minor disruptions of the neovolcanic zone along the Mid-Atlantic Ridge (contour interval = 100 m). Stippled pattern indicates volcanic edifices which we interpret as belonging to the neovolcanic zone, dashed lines mark the location of the neovolcanic zone.

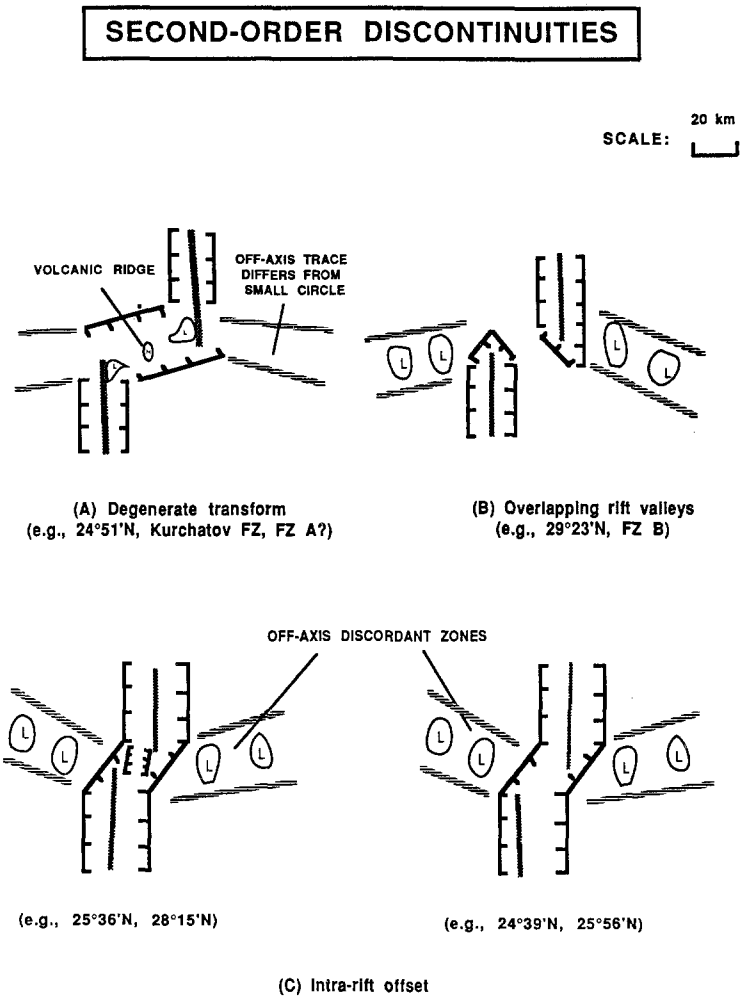

Fig. 12. Schematic characteristics of second-order discontinuities along the Mid-Atlantic Ridge between 24°00′ N and 30°40′ N. Three main types of second-order discontinuities are recognized. (A) Large non-transform offsets (>20 km) are reminiscent of transform faults, but a sustained strike slip fault is not maintained at these offsets. Axis-parallel volcanic ridges may be present within the intra-offset area. These ridges may be the result of extension between the offset neovolcanic zones. (B) Overlapping rift valleys. (C) *En échelon* jog with and without an extensional basin between the offset spreading axes. Bathymetric highs and lows are indicated by Hs and Ls.

magmatic processes. Wide, U-shaped segments (Group II) are associated with less robust volcanism, widespread tectonic activity, and the absence of circular mantle Bouguer anomalies. These segments may be dominated by amagmatic processes. The full spectrum of observed rift valley morphologies, which is only approximated by our bimodal classification, may be accounted for by variations in the volume, distribution and temporal continuity of magmatic upwelling between segments, and by the episodic nature of volcanic activity superposed on nearly-continuous extension at the plate boundary.

4.2. Intra-segment, volcano-tectonic variability

Our study of the Mid-Atlantic Ridge reveals common patterns of morphotectonic variations within each spreading segment irrespective of their first-order morphology. Within each segment, the inner valley floor is narrowest where the spreading center is shallowest. The inner floor widens by as much as 10–15 km and deepens by as much as 500 m near the discontinuities which bound the segments. Similar observations have been made for the MAR in the

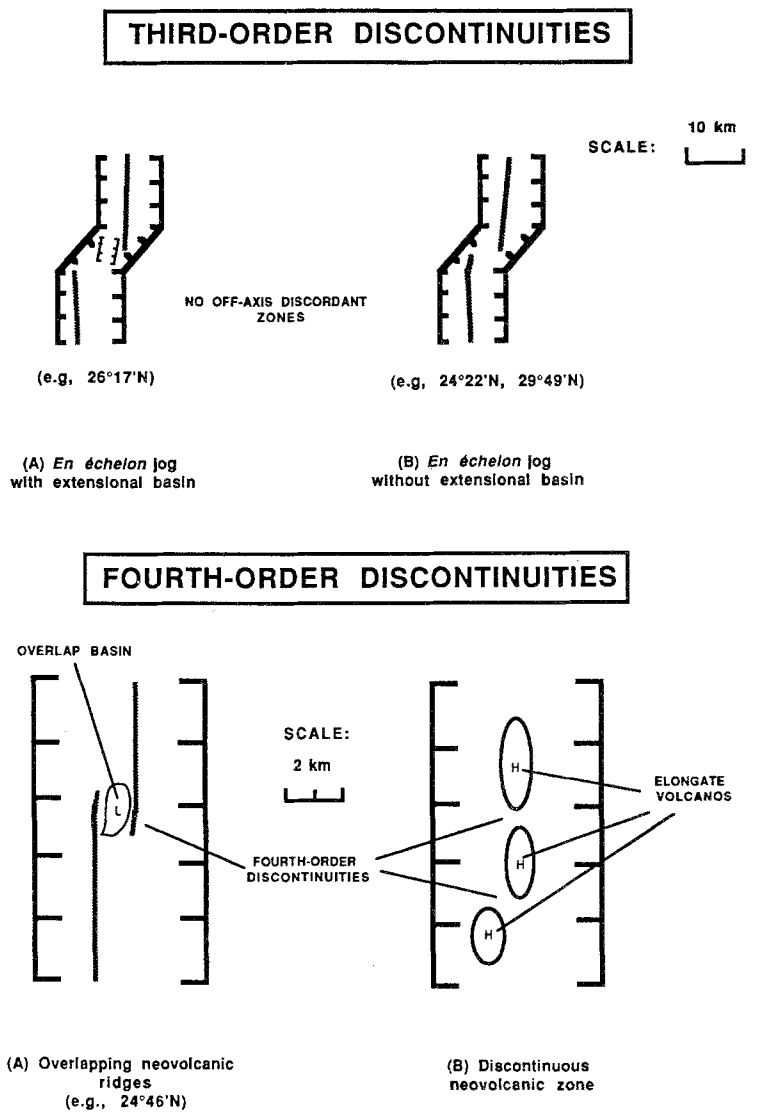

Fig. 13. Schematic characteristics of third- and fourth-order discontinuities along the Mid-Atlantic Ridge between 24°00′ N and 30°40′ N. Two main types of third-order discontinuities are recognized: (A) *En échelon* jogs accommodated by an extensional basin between the offset spreading axes, (B) *En échelon* jogs. Two main types of fourth-order discontinuities are recognized: (A) Overlapping neovolcanic ridges, (B) *En échelon* volcanoes. Bathymetric highs and lows are indicated by Hs and Ls.

FAMOUS area (Crane and Ballard, 1981) and the Juan de Fuca Ridge (Barone and Ryan, 1988). Along-axis variations in the size of the rift valley can be explained by along-axis variations in the thickness of the brittle lithosphere at the axis (Phipps Morgan *et al.*, 1987; Sempéré, 1991). The widening of the rift valley away from segment mid-points may be accounted for by the deepening of the brittle ductile-transition zone, such as is observed along the 25°56′–26°17′ N segment (Kong *et al.*, 1992). Thus, intra-segment variations in the dimensions of the rift valley reflect the three-dimensional thermal structure of the axial lithosphere and the geometry of mantle upwelling beneath the spreading center (Sempéré, 1991).

The NVZ usually corresponds to the shallowest part of the inner valley and is often associated with a ridge flanked by marginal lows. The NVZ is in general more robust near the segment mid-points than near their ends (Figures 6a–9a). It looses definition and becomes discontinuous near the ends of each segment, although exceptions to this rule do occur (Figures 4a, 7a, 10a). The NVZ and marginal lows deepen systematically toward the discontinuities. The NVZ may encompass the entire inner floor near the middle of segments that are extremely active

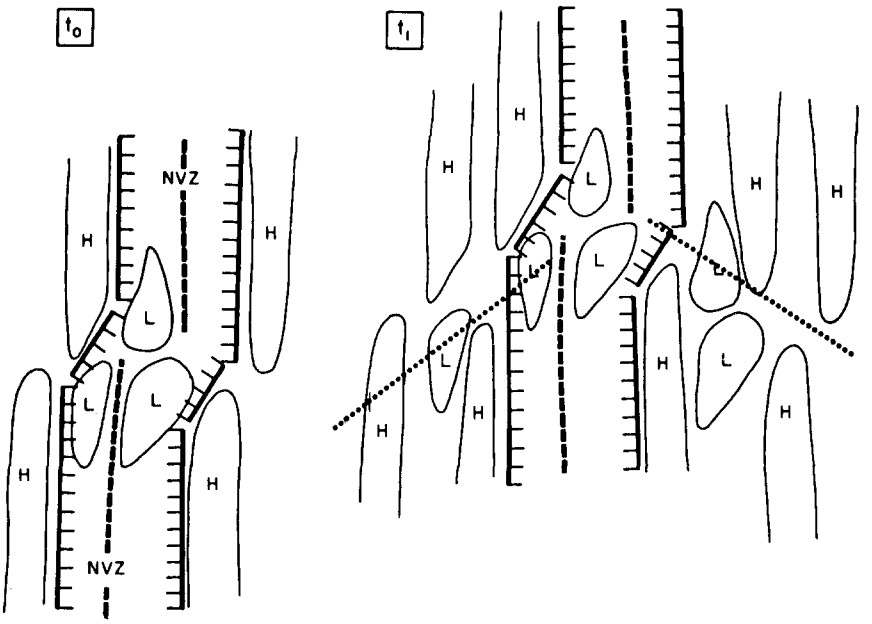

Fig. 14. Model of the evolution of non-transform discontinuities and the creation of off-axis discordant zones. Isolated basins (Ls) which form the off-axis traces of second-order discontinuities may be the fossil expression of the terminal lows which flank the neovolcanic zone near the ends of each segment. The starting configuration (t_0), especially the location of the terminal lows, and the evolution of the discontinuity are one of several possibilities. In this example, the southern segment has migrated north and the south end of the northern segment has retreated north. Dotted line represents the off-axis traces of the discontinuity.

magmatically. This may be the case of the 24°51′ N–25°36′ N segment.

The faults which bound the rift valley are more continuous and linear in the center of segments, where the rift valley is shallowest, than near their ends. The rift valley is usually symmetric near the mid-point of each segment. Away from the middle of segments, the rift valley is in general asymmetric: the steeper and more elevated side is created by a few fault zones with throws > 500 m while the relief of the gentler, less elevated side is composed of a staircase of small faults (Figures 3b–10b). The ridges which form the rift mountains tend to be shallowest and broadest near the latitude of the segment mid-point. These ridges taper off toward the discordant traces of the discontinuities.

The above morphotectonic characteristics, observed to varying extents within all segments, define an intra-segment variability which is superposed on the inter-segment variability discussed previously. The intra-segment variability may reflect differences in the relative importance of magmatism, tectonism and dynamic uplift along strike away from a zone of enhanced magma upwelling near the mid-point of each segment, and may reflect variations in the thermo-mechanical structure of the axial lithosphere at the segment scale. The contribution of magmatism to the morphology will be more important near the shallowest portion of the rift valley within each segment than near the segment ends. Conversely, the relative contribution of tectonic (amagmatic) extension to the morphology will become more important toward the discontinuities. The fact that teleseismic earthquake swarms occur predominantly near the ends of spreading segments supports this idea (Bergman and Solomon, 1990; Lin and Bergman, 1990).

5. Discussion

5.1. Structure of the rift valley

The rift valley of the Mid-Atlantic Ridge is an ubiquitous feature in the North Atlantic away from Iceland. The apparent two-dimensionality of the rift valley has often been interpreted as reflecting a symmetric arrangement of faults about the axis of accretion. However, this two-dimensionality is misleading because, at the segment scale, the rift valley is in general asymmetric. Away from the segment mid-points, one flank of the rift valley is usually steeper and more elevated than the other one. The relief of

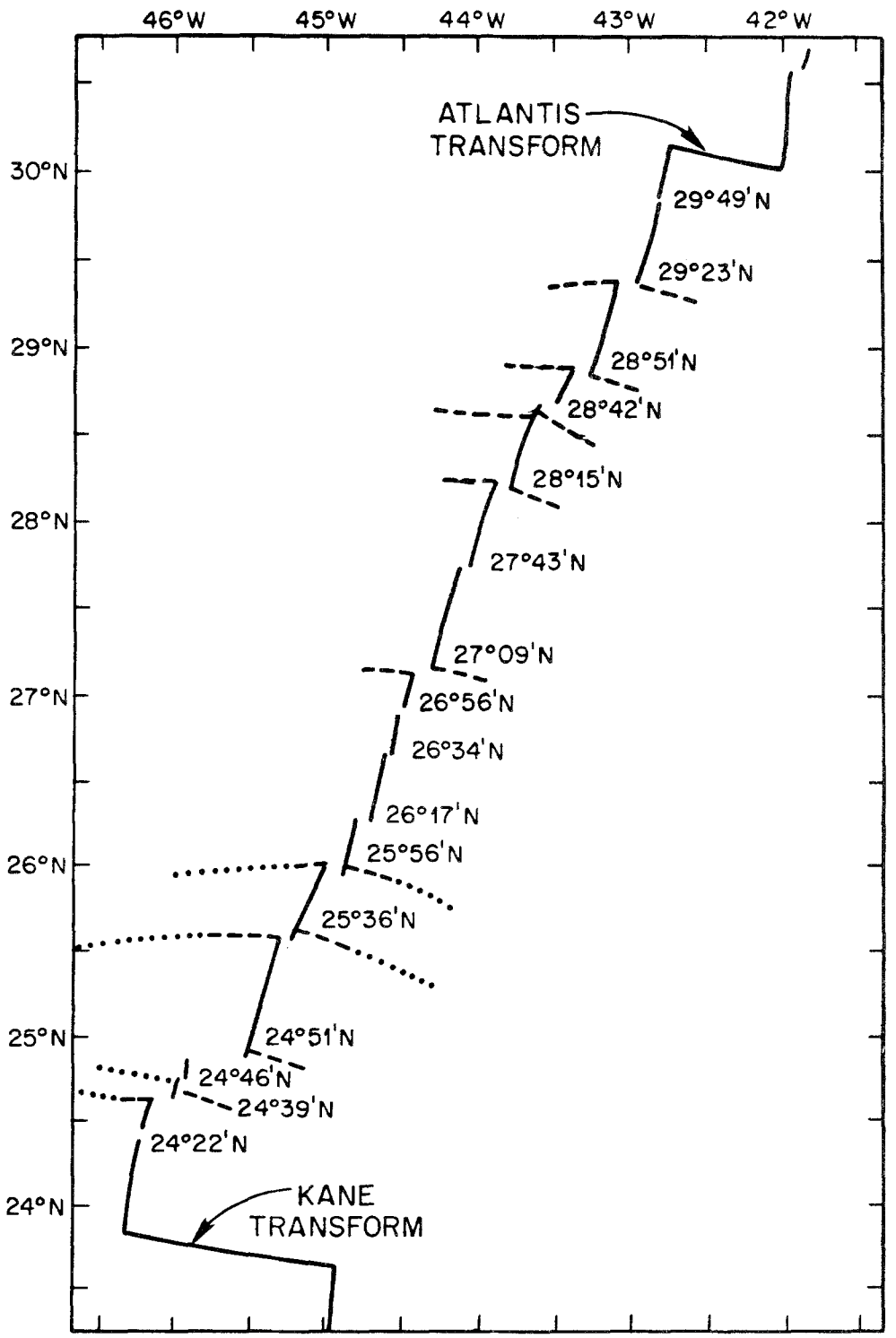

Fig. 15. Off-axis discordant zones associated with non-transform discontinuities between the Kane and Atlantis Transforms. Thick stippled lines indicate the spreading segments, dashed lines indicate the off-axis traces interpreted from our coverage, dotted lines indicate the traces based on narrow-beam bathymetry further off-axis (Rona, 1976; Rona and Gray, 1980).

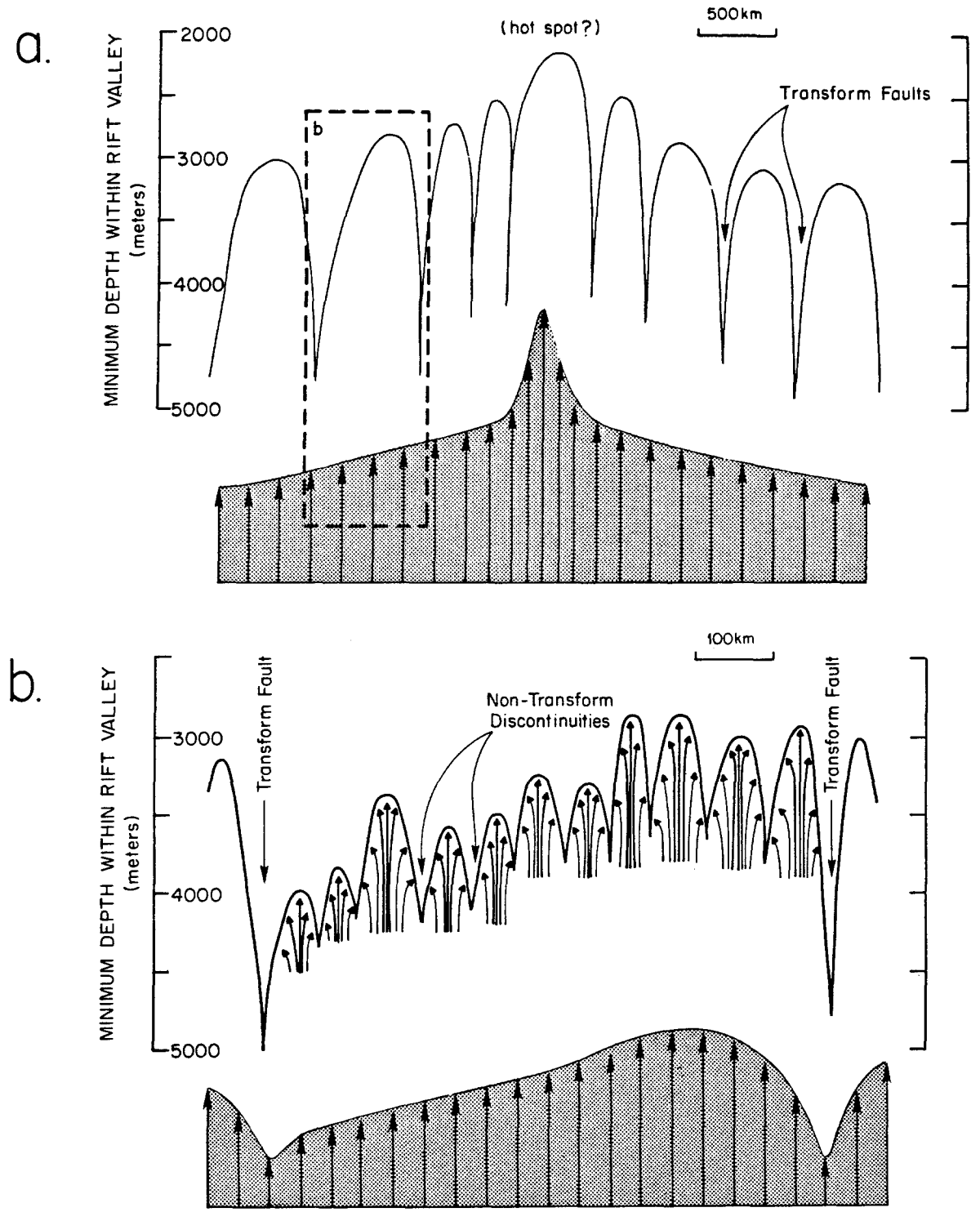

Fig. 16. Model for the segmentation of the Mid-Atlantic Ridge. (a) the very long-wavelength variations in the depth of the MAR (1000–5000 km) are strongly influenced by upwelling from the deep mantle (LeDouaran and Francheteau, 1981), possibly related to hot spots, and may correspond to the deepest-level segmentation. Dashed box corresponds to lower diagram. (b) The long-wavelength undulations (200–1000 km) in the depth of the spreading center may reflect the upwelling of asthenospheric material between transform faults. Decompression melting of the upwelling asthenosphere may lead to distinct, magmatic upwelling events, which will feed distinct spreading segments. The surficial expression of this smaller length scale segmentation (20–80 km) is defined by non-transform discontinuities. Within each spreading segment, magmatic upwelling will be enhanced where the spreading center is shallowest.

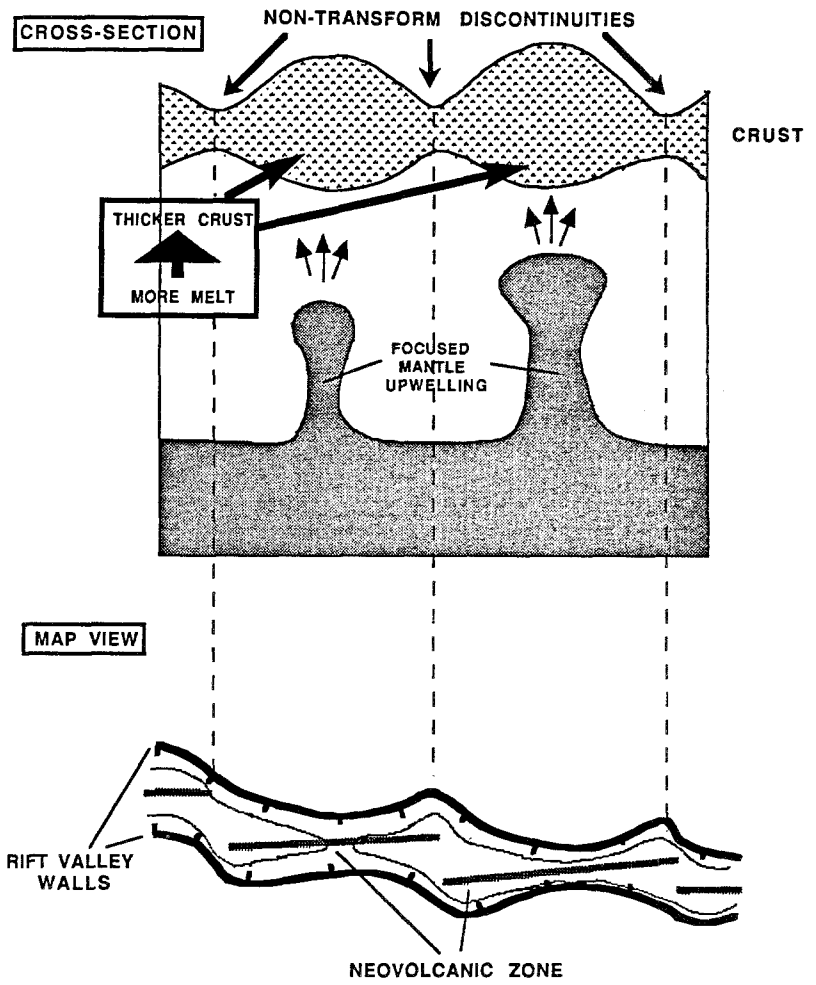

Fig. 17. Cross-section and map view of two spreading segments associated with circular, mantle Bouguer gravity anomalies. Diagrams are schematic and not to scale. Focused mantle upwelling beneath the middle of each segment will result in enhanced melting and thicker than usual crust away from the bounding discontinuities.

the more elevated side is achieved by a few, large-throw (> 500 m) faults, while the less elevated flank is associated with a gradual ramp of terraces bounded by small-throw faults. Thus, half-grabens may be important features along the rift valley of the MAR (Figure 19).

This situation bears some resemblance to that of the East African Rift (EAR) which is also asymmetric in cross-section as a rule (i.e., Rosendahl, 1987; Ebinger, 1989a, b; Ebinger *et al.*, 1989; Karson and Curtis, 1989). Half-grabens along the EAR often consist of 50–100-km-long units bordered on one side by 2–5-km-high border faults and, on the other side, by lower-relief, faulted monoclines or ramps (Rosendahl, 1987). The major bounding faults are arcuate in plan form (Rosendahl, 1987; Ebinger, 1989a, b; Ebinger *et al.*, 1989). Adjacent half-grabens along strike are linked by oblique-slip, transfer faults which accommodate differential throws and horizontal offsets between adjacent extensional basins (Ebinger, 1989b). Full-grabens may be a result of linking together of half-grabens (Rosendahl, 1987). Along the eastern branch of the African Rift, volcanoes lie near the center of half-grabens (Karson and Curtis, 1989). Thus, the EAR appears to be segmented into half-grabens bounded by transfer faults (Ebinger, 1989a, b), perhaps as the result of upwelling mantle diapirs beneath individual rift basins (Karson and Curtis, 1989). The EAR and the MAR are not directly comparable though because the asymmetry in the rift valley of the MAR is more pronounced near the segment ends, contrary to what is observed along

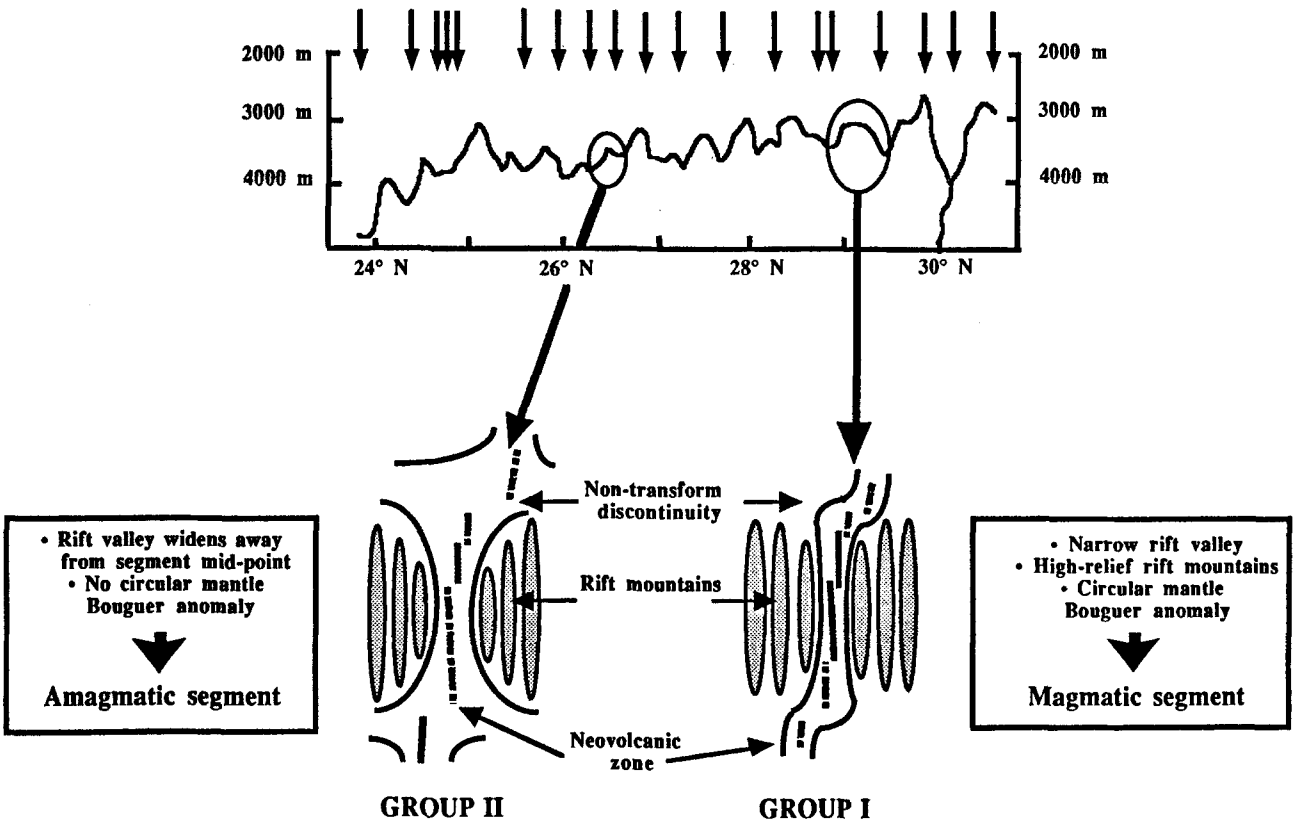

Fig. 18. Schematic morphology of Group I and Group II segments.

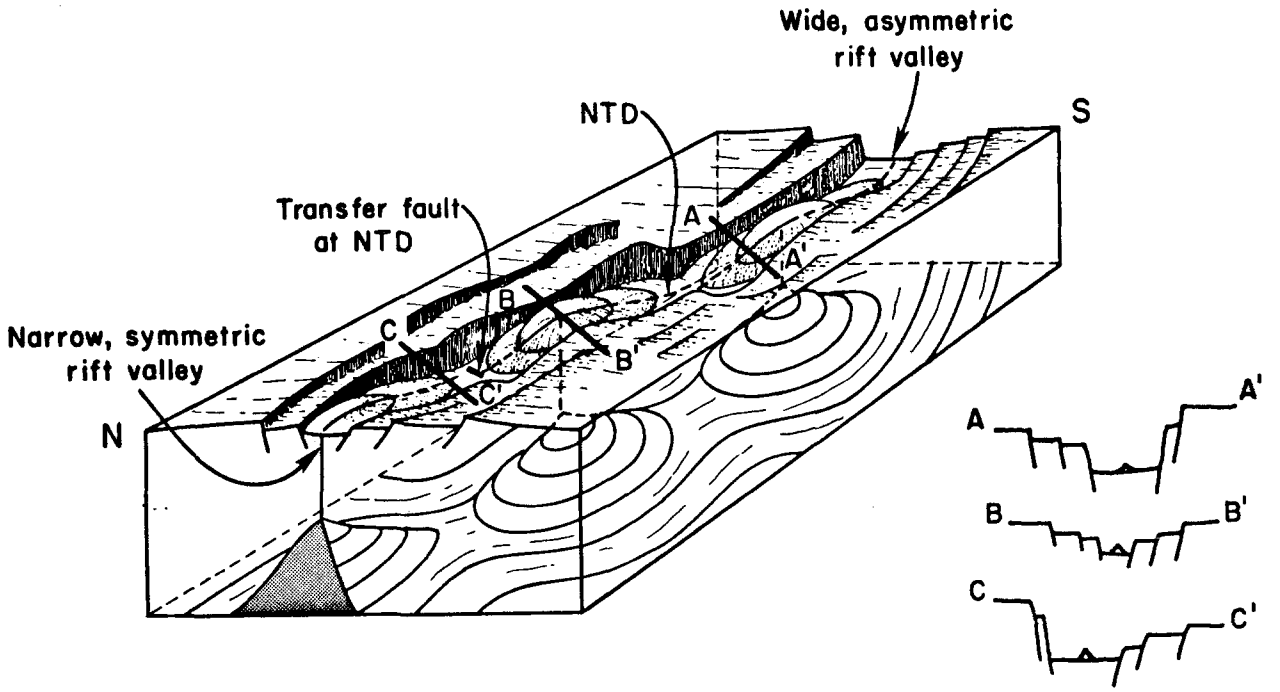

Fig. 19. Schematic block diagram of the Mid-Atlantic Ridge (modified from Karson and Curtis (1988)) outlining the relationship between variations in the pattern of faulting within segments, half-graben structures, and zones of enhanced mantle upwelling beneath segment mid-points.

the EAR. Along the MAR, the detachment faulting, which is presumably the cause of the rift valley asymmetry, is more developed near spreading center offsets (i.e., Karson and Dick, 1983).

5.2. Formation of abyssal hills

Kappel and Ryan (1986) explained the generation of rift-flanking topography on the flank of the Juan de Fuca Ridge by a cyclic process in which the construction of a crestal ridge within the rift valley is followed by the collapse and splitting of the summit region of this ridge. The two halves of the split construction form two abyssal hills which are fault-bounded on their axis-facing side. Pockalny *et al.* (1988) and Kong *et al.* (1988) noted the similarity between the neovolcanic ridge found in the inner valley of the MARK area and ridges present in the rift mountains. They suggested that the ridges formed in the inner floor and that they were transported out of the rift valley without significant dismemberment.

Our study provides further constraints on the mechanisms of abyssal hill formation. A key observation is that, in a few segments within our coverage, the rift mountain ridges increase in length and height away from the axis, before subsidence and sedimentation diminish the apparent sizes of these edifices further off-axis. This pattern is especially apparent in the 24°51′–25°36′ N segment (Figure 4a). There, the second and third ridges away from the axis appear progressively more elevated and longer than the previous ones (Figures 20). All ridges are bounded on their axis-facing side by a small-throw fault which can be traced for nearly the entire length of the segment (Figure 20).

There are at least two ways to explain this observation. The first one assumes that the hypothesis of Pockalny *et al.* (1988) is correct and that ridges in the rift mountains were created as neovolcanic ridges within the inner floor of the rift valley. The observed increase in the size of the ridges away from the axis would indicate a decrease in the magmatic budget of the segment in the last 2 Ma. Although this hypothesis cannot be refuted on the basis of the data we have collected, it does not take into account all the observations in the case of the 24°51′–25°36′ N segment. In particular, it does not account for the fact that even the ridges closest to the axis appear to be bounded on their axis-facing sides by faults which extend beyond the length of the ridges for nearly the entire extent of the segment.

The second hypothesis, based on the work of Kappel and Ryan (1986), is our preferred one. The spatial relationship between the shallowest part of the inner floor and the shallowest part of the off-axis ridges suggests that the relief of the central part of the ridges is, to a large extent, the result of volcanic construction within the inner floor, the remainder being due to tectonic uplift. The small sizes of the axis-facing faults which bound the ridge closest to the axis attest to this origin. These bounding faults can, in general, be traced along the entire segment length, even where there is no evidence for an off-axis, bathymetric ridge per se (Figure 20). The apparent lengthening of rift mountain ridges away from the axis may occur by uplift along the axis-facing faults which flank the ridges near their ends (Figure 21). As new lithosphere is accreted at the axis, the small ridge immediately close to the axis will be tectonically lengthened by extension near the segment ends (Figure 1). Ridges in the rift mountains may thus be broken into two components: one which corresponds to their middle section and which is mostly due to volcanic construction at the inner floor saddle, one which corresponds to their ends and which is mostly of tectonic origin. Thus, we propose that ridges in the rift mountains are created by a combination of tectonic and volcanic, and not mainly volcanic processes. This hypothesis predicts that only the axis-facing side of the ridges which flank the rift valley should be fault-bounded. Our interpretive cross-sections of the rift valley support this assertion (Figure 20), but the inadequacy of Sea Beam data to differentiate between fault-bounded structures and steeply-dipping volcanic constructions requires the use of near-bottom systems to unambiguously test this hypothesis.

The above model accounts for the apparent lengthening of rift mountain ridges away from the axis. Such lengthening is not observed in all segments and, subsequently, the model that we have outlined is not necessarily valid everywhere. This model also does not account for abyssal hills whose side facing away from the axis is fault bounded. Thus, we cannot conclude in terms of a unique model for the formation of abyssal hills along the MAR. The models of Kappel and Ryan (1986) and Pockalny *et al.* (1988), and the one that we have

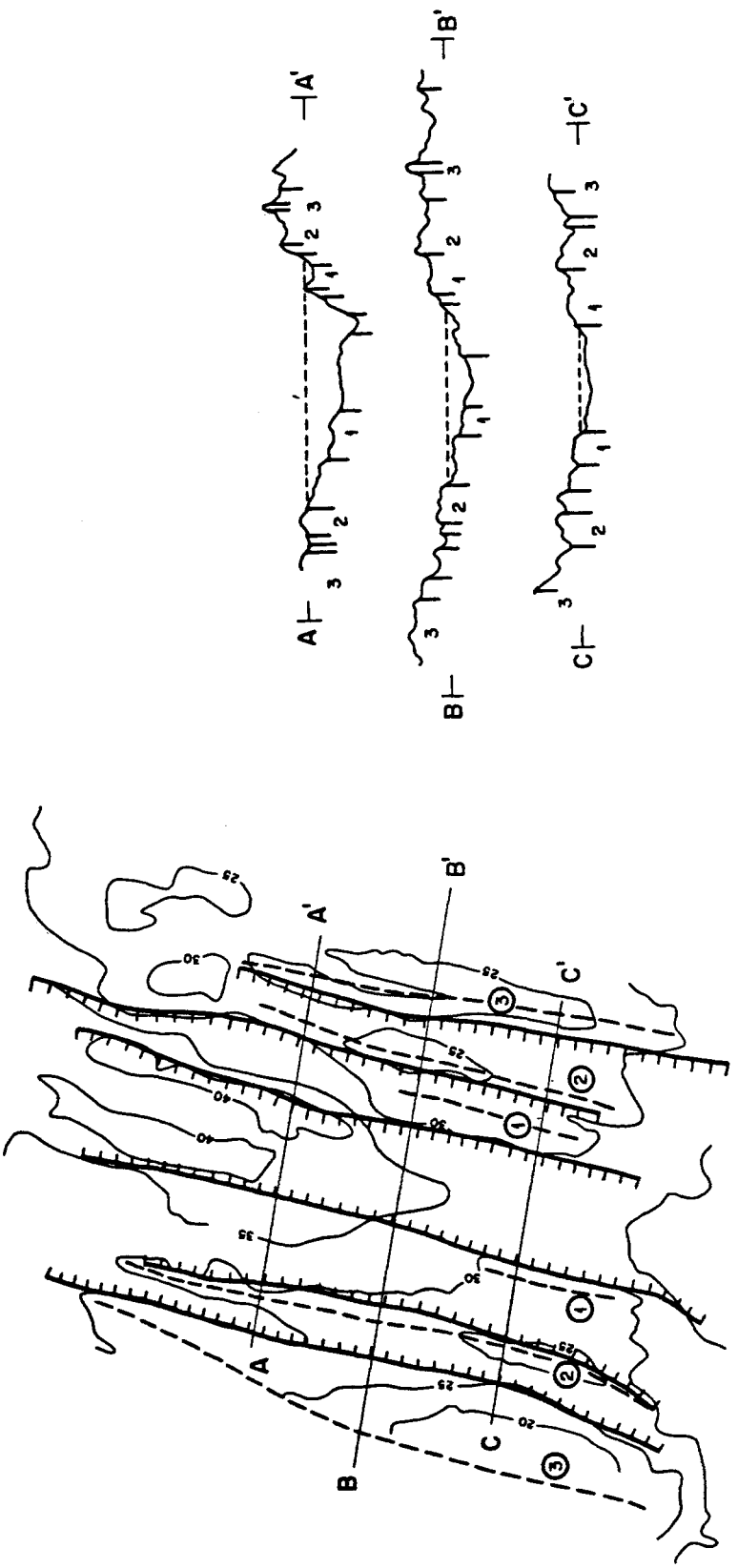

Fig. 20. (a) Schematic diagram of the 24°51′–25°36′ N segment. Note that the bathymetric expression of the ridges which form the rift mountains increases in length and height away from the axis. Note also that these ridges, even the short one closest to the axis, appear bounded on their axis-facing sides by faults which extend for nearly the entire length of the segment. (b) Bathymetric profiles across the 24°51′–25°36′ N segment.

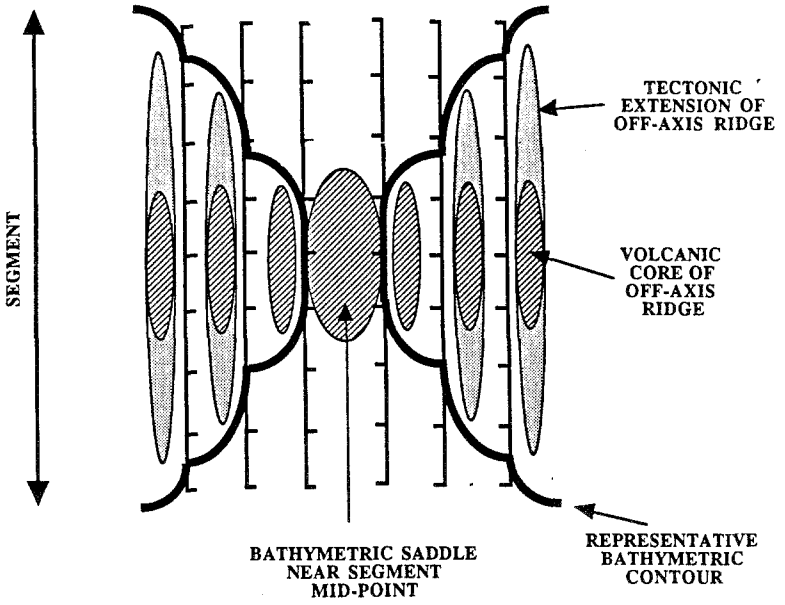

Fig. 21. Schematic representation of the formation of abyssal hill topography. The core of the ridges in the rift mountains is the result of volcanic processes occurring in the rift valley. These initially short ridges are bounded by axis-facing faults which extend for the entire length of the segment, and are tectonically lengthened by enhanced amagmatic extension at the ends of segments.

outlined above, may be valid only in the simplest cases. The complexity of the rift mountain terrain in some segments within our coverage precludes a simple, cyclic mechanism for the generation of abyssal hill topography.

5.3. Architecture of the oceanic crust

Our model of the segmentation of the MAR assumes that the availability of melt is enhanced beneath the shallowest portion of the inner valley floor, approximately midway within each segment, and that it is diminished beneath the discontinuities which bound the segments. Since variations in melt availability away from a locus of enhanced upwelling could result in along-strike, crustal thickness variations, non-transform discontinuities, like transform faults, may be associated with large disruptions in the structure of the oceanic crust, even if they have small lateral offsets.

Seismic refraction experiments (Detrick *et al.*, 1982; Cormier *et al.*, 1984; Sinha and Louden, 1984) have revealed that Atlantic transforms are commonly, but not always, associated with anomalous crustal structures. Crust found at these large transforms is often very thin and characterized by low seismic velocities, the absence of a layer 3 refractor and a well-developed crust-mantle boundary. Gravity studies (e.g., Louden and Forsyth, 1982; Prince and Forsyth, 1988) are consistent with crustal thickness variations beneath some Atlantic fracture zones.

Seismic experiments over small offsets of the MAR and their off-axis traces indicate that they may also be associated with anomalous crustal structures. Unfortunately no such data are presently available for our survey area. Seismic reflection and expanding spread profile data across the 20-km-offset, Blake-Spur F. Z. in 135-Ma-old crust in the North Atlantic reveal that the crust-mantle boundary may be elevated to unusually shallow depths (2–2.4 km) beneath this discontinuity (Mutter *et al.*, 1984, 1985; NAT Study Group, 1985; McCarthy *et al.*, 1988; Minshull *et al.*, 1991). Steeply-dipping, mafic-ultramafic cumulates, which are best developed in the center of ridge segments, seem to disappear as the crust thins toward the Blake Spur offset (McCarthy *et al.*, 1988). Likewise, a seismic refraction experiment over the trace of a ~15-km offset of the MAR in 40–50 Ma lithosphere reveals a narrow zone of anomalous crust, less than 7 km in width, where layer 3A appears to be missing and the crust appears to be thinner than normal (White and Matthews, 1980). Finally, the 23°15′ N Discontinuity (MARK area) corresponds to a seismic boundary

which separates 6–7 km-thick crust with normal crustal and upper mantle velocities to the south, and 4–5-km-thick crust with no distinctive layering to the north (Purdy and Detrick, 1986). This non-transform discontinuity and its off-axis trace are associated with a gravity high, suggesting that systematic crustal thickness variations have been associated with the northward migration of the offset for the past 3–4 Ma (Morris and Detrick, 1991).

Gravity data, where available in our survey area, are consistent with our model of the segmentation of the MAR. Between 27°50′ N and 30°40′ N, circular gravity lows over the middle of each segment and gravity highs over the bounding discontinuities are apparent in a contour map of the mantle Bouguer anomaly. Lin *et al.* (1990) postulated that the collective effects of along-axis variations in crustal thickness and density in the shallow mantle, both due to focused mantle upwelling beneath segment mid-points, are the sources of the gravity anomalies. Enhanced melting and high mantle temperatures beneath segment mid-points may result in a negative density contrast at depth and cause negative gravity anomalies. However, the gravity signal due to buoyant upwelling is likely to be small (Lin and Phipps Morgan, 1992). Enhanced melting will also result in the emplacement of thicker crust in the middle of each segment and cause negative gravity anomalies (Figure 17). If crustal thickness variations are the sole source of the anomalies, gravity data are consistent with up to 50% change in crustal thickness within some of the segments (Lin *et al.*, 1990). Mantle Bouguer lows are more marked for the longer spreading segments, indicating that long segments may be associated with larger buoyancy-driven mantle plumes and a larger degree of decompression melting, and resulting thicker crust, beneath their mid-points (Lin *et al.*, 1990). Amagmatic extension may be responsible for additional crustal thinning near the segment ends (Karson *et al.*, 1987; Harper, 1988; Norrell and Harper, 1988) and for the exposure of deep-level rocks along the rift valley wall (e.g., Karson *et al.*, 1987).

In addition to variations in thickness due to a reduced melt supply away from a localized zone of magma upwelling, the structure of oceanic crust beneath non-transform discontinuities may be fundamentally different than it is beneath the segment mid-points. We expect that in the center of spreading segments, above the zone of maximum melt production, oceanic crust will reflect the presence of transient magma chambers and will exhibit a distinctive layering. Near the ends of segments, where we postulate that melt production is at its lowest, oceanic crust may be highly heterogeneous, reflecting the past presence of ephemeral magma bodies, or it may only consist of a thin basaltic layer overlying abyssal peridotites (Nicolas, 1985; Dick, 1989). In the latter case, the absence of a gabbroic layer would reflect the lack of magma chamber and imply lateral flow of melt away from the segment mid-points toward the discontinuities (Dick, 1989).

Our observations show that the response of the lithosphere to local and regional stresses along the MAR results in an approximately symmetric pattern of faults near segment mid-points, and an asymmetric pattern toward segment ends. Since regional stresses are not expected to vary significantly over the scale of a segment, differences in faulting must be the result of variations, at the segment scale, in near-field lithospheric stresses, and/or in the mechanical response of the lithosphere to this stress field. A corollary of a model of enhanced mantle upwelling is that the thermal structure of the lithosphere near the axis and the crustal structure vary along-strike within each segment. Along-axis variations in lithospheric structure and temperature will modify the mechanical response of the plate to stresses, and may explain the varying pattern of faulting observed at the segment scale. Variations in the structure of oceanic crust along the axis of the spreading center have been studied during a microseismic experiment within the 25°56′–26°17′ N segment (Kong *et al.*, 1992). Kong (1990) suggested that the along-axis high of this segment may have been the site of a recent episode of magmatic intrusion. Microearthquakes occurred at shallower focal depths (usually <3.5 km) beneath the along-axis high than beneath the along-axis deep 15 km to the south (5.4 ± 1.0 km). Thus, the brittle-ductile transition appears ~ 2 km deeper near the ends of the 25°56′–26°17′ N segment than near its shallow middle. Since the geometry of faults is partly controlled by their depth, these results suggest that distinct faulting regimes affect the middle and ends of a given segment, a result consistent with our observations. Thus, along-axis variations in the thermal structure of the axial lithosphere, possibly associ-

ated with focused mantle upwelling, may account for some of the observed morphotectonic patterns at the segment scale (Sempéré, 1991).

Conclusions

Analysis of Sea Beam bathymetric data along the MAR between 24°00′ N and 30°40′ N reveals the segmentation characteristics of this slow-spreading center, and provides insights into the processes that cause the segmentation of the plate boundary. Our results support the following conclusions:

(1) The spreading center is segmented at a scale of 10–100 km by transform and non-transform discontinuities. These offsets generally occur at along-axis depth maxima. Non-transform discontinuities are accommodation zones which allow adjacent spreading segments with different tectonic styles and levels of magmatic activity to coexist. At non-transform discontinuities, the horizontal shear between the offset ridge segments is not accommodated by a narrow, sustained shear zone. The morphology of non-transform discontinuities covers a broad spectrum which is partly controlled by the offset distance between adjacent segments.

(2) The larger non-transform discontinuities are associated with off-axis discordant zones in the form of isolated, but spatially aligned, basins. These basins may be the fossil expressions of the terminal lows which bound the neovolcanic zone near the ends of each segment. For lithosphere less than 2 Ma in age, the off-axis traces appear to form north-pointing lineaments.

(3) The morphotectonic characteristics of the spreading center are the result of the superposition of an intra- and an inter-segment variability. The inter-segment, morphotectonic variability may reflect differences in the volume, focusing and temporal continuity of magmatic upwelling between segments. The intra-segment, morphotectonic variations may represent differences in the relative importance of volcanism and tectonism along strike away from a zone of enhanced magma upwelling within each segment. Along-strike variations in the tectonic characteristics of segments may be the result of along-axis variations in mechanical structure and local stress field. The rift valley of the MAR is asymmetric away from segment mid-points. Half-grabens may be the fundamental unit of the rift valley.

(4) Analysis of gravity data within our survey area suggests the presence of zones of enhanced mantle upwelling beneath the mid-point of some of the segments. Non-transform discontinuities may be associated with crustal thinning away from upwelling zones. The pattern of segmentation and along-axis morphotectonic variations of the spreading center are consistent with this interpretation. A simple morphotectonic classification of segments yields two primary groups. The presence, or absence, of a zone of focused mantle upwelling beneath the segment mid-point and/or variations in crustal structure appear to partly control the morphology of segments.

Acknowledgements

We are very grateful to J. Miller, J. Dolan and R. Edwards for their help in the acquisition and processing of the Sea Beam data. We are also indebted to Captains Peterlin and O'Loughlin and the crew of the R/V Robert D. Conrad, R. Batholomew, W. Robinson, F. Robinson, G. Christensen, M. Montfort, J. Palmer, B. Trams, C. Wolfe, and C. Zervas. We benefitted from discussions with R. Detrick, J. Fox, J. Francheteau, L. Géli, K. Macdonald, P. Patriat, R. Pockalny, S. Tighe and C. Zervas, and from the careful reviews of two anonymous reviewers. We thank N. Grindlay and J. Karson for preprints ahead of publication. L. Sylvester drafted the figures. This research was supported by the National Science Foundation (contracts OCE-8722980 and OCE-9000285).

Appendix: Spreading Segments and Spreading Center Discontinuities Between 24°00′ N and 30°40′ N

The Kane-24°22′ N segment

This 57-km-long segment is associated with an hourglass rift valley (Figure 3a). The shallowest point within the inner valley floor is found near 24°06′ N at a depth of 3950 m. The inner valley is narrowest near this latitude. It widens and deepens gradually to the north and south. The east and west valley wall strike 007° north of the saddle, and 015° and 025° respectively south of it. The rift valley is symmetric near the axial saddle (profiles J–J′ to L–L′, Figure 3b) but asymmetric elsewhere. Near the western Kane ridge-transform intersection (RTI; Karson and Dick, 1983;

Pockalny *et al.*, 1988) and the 24°22′ N Discontinuity, the east wall is steeper than the west one (profiles M–M′, N–N′ and I–I′). The east wall consists of 1–3 large throw (>500 m) fault zones. This result is confirmed by the submersible transect of Zonenshain *et al.* (1989) near 23°50′ N. South of the saddle, the poorly-developed NVZ corresponds to a string of volcanic edifices which cuts across the RTI (Figure 3a) (Karson and Dick, 1983). North of the saddle, the NVZ is of intermediate strength and consists of volcanic edifices which integrate to form a discontinuous, 50–150-m-high ridge trending 010°.

The 24°22′ N discontinuity

The 24°22′ N discontinuity corresponds to a right-stepping, ~1-km offset of the NVZ (Figure 3a). Because it is associated with a large, along-axis depth anomaly (500–900 m) and a drastic change in the morphology of the NVZ and of the rift valley, we interpret it as a major discontinuity. The inter-segment area is devoid of any obvious structural elements, including a narrow, strike-slip fault zone, resolvable with Sea Beam. The absence of discordant zones on the flanks of the discontinuity (Figure 3a; Rona, 1976) indicates that it has not existed for a long time, or that it has not been associated with a large offset and depth anomaly in the past. There are no offsets in the Brunhes–Matuyama (B–M) boundary near 24°22′ N (Sempéré *et al.*, in prep.), confirming that, 0.72 Ma ago, the discontinuity either did not exist or was not associated with an offset resolvable by inversion of surface magnetic anomalies.

The 24°22′–24°39′ N segment

The overall trend of the MAR between 24°30′ N and 25°00′ N is 057°, 45° oblique to the average spreading direction between the Kane and Atlantis Transforms (Argus *et al.*, 1989). The 35-km-long 24°22′–24°39′ N segment lies within this oblique portion of the MAR (Figures 3a). The west and east wall of the inner floor consists of 300–700-m-high scarps striking 010°–045° and 025°–075°, respectively. The 10-km-wide rift valley is approximately symmetric (profiles E–E′ to H–H′, Figure 3b). The mean depth of the rift mountains is ~3200 m, compared to ~2700 m for the segments north of 25°00′ N and south of 24°30′ N. The robust NVZ is located on top of a 400–600-m-high ridge which extends for the entire length of the segment along a strike of 018°. The ridge is shallowest (3550 m) near 24°37′ N and deepens to 4000 and 4450 m at its north and south end respectively. Numerous volcanic peaks are superposed on this ridge. This result is confirmed by a submersible transect near 24°23′ N (Zonenshain *et al.*, 1989).

The 24°39′ N discontinuity

The MAR is offset by ~14 km in a right-stepping manner near 24°39′ N (Figure 3a). This non-transform offset is associated with a clockwise change of 7° in the orientation of the NVZ, and a 5-km, right stepping jog of the east valley wall near 24°33′ N. The inter-segment area is characterized by a ~4500-m-deep basin east of the southern NVZ. On the west flank, near 24°39′ N, 46°20′ W, we observe a basin which lies along an azimuth of 270°–315° away from the tip of the southern NVZ. On the east flank, two basins, centered near 24°36′ N, 45°55′ W and 24°38′ N, 45°48′ W, integrate to form a 085–115° lineament. The presence of V-shaped, off-axis traces indicates that the 24°39′ N Discontinuity has persisted with time, but that strike-slip faulting has not been sustained within a narrow zone at this locality. These results are in agreement with those of Rona (1976).

The 24°39′–24°46′ N segment

The rift valley of this 13-km-long segment is flanked by low-relief (400–1000 m) rift mountains (Figure 3a). The west valley wall consists of 200–600-m-high scarps which trend ~040°. The east wall, which is made up of 300–500-m-high scarps trending ~020–040°, is somewhat steeper and more elevated (profiles C–C′ and D–D′, Figure 3b). The faulted blocks which form the rift mountains do not display a lineated fabric. The NVZ is located on top of a 400-m-high ridge which extends between 24°39′ N and 24°45′ N along a strike of 025°. We classify this NVZ as robust. It is superposed by small, subcircular volcanic peaks 50–100 m high.

The 24°46′ N discontinuity

Near 24°46′ N, the MAR is offset by 3 km in a right-stepping manner (Figures 3a). There is no evidence for a strike-slip fault linking the offset strands of the NVZ (Figure 11). Instead, the offset NVZs overlap by ~3 km and are separated by a 200-m-deep depression. As the ridges overlap, they curve

toward one another. There is a change of 6° in the orientation of the NVZ across the discontinuity. We cannot identify any structures on the flanks which may mark the trace of the discontinuity in older seafloor.

The 24°46′–24°51′ N segment

This 10-km-long segment is flanked by low-relief (400–1000 m) rift mountains (Figure 3a). The west wall of the rift valley consists of 200–600-m-high scarps trending ~040°, the east wall of 500–900-m-high scarps trending ~015–045°. The rift valley is asymmetric: its east flank is steeper than the west flank (profiles A–A′ and B–B′, Figure 3b). The rift mountains consist of faulted blocks which do not form the lineated topography often found on the flanks of the MAR. The robust NVZ is located on top of a 400-m-high ridge which extends between 24°45′ N and 24°50′ N along a strike of 026°. The shallowest point (3600 m) in this segment is found along the NVZ (24°48′ N).

The 24°51′ N discontinuity

The axis of the MAR is offset by 30 km in a right-stepping manner near 24°51′ N. The offset area is associated with two basins and an intra-offset ridge. The first basin is a 4450-m-deep, triangular low which flanks the northern NVZ south of 25°00′ N and which is bounded to the south by a 500–1000-m-high wall striking ~100° (Figure 4a). The 300-m-high intra-offset ridge extends along a strike of 026° between 24°49′ N, 45°42′ W and 24°53′ N, 45°41′ W near the southwest corner of the triangular basin. The second basin is a Γ-shaped, 4700-m-deep low which lies west of the intra-offset ridge. Thus, the discontinuity may be accommodated by two *en échelon* shear zones, parallel to the spreading direction. One of these shear zones may extend along the south margin of the basin between the northern NVZ and the intra-offset ridge; the other may link the south tip of the intra-offset ridge to the southern NVZ near 24°50′ N. The intra-offset ridge may be the result of volcanism associated with the extensional jog of the shear zones.

The discontinuity is associated with 3400–3800-m-deep basins which integrate spatially to form a 095–115° trough on the east flank of the spreading center. Rona (1976) obtained an orientation of 107° for this lineament. The few basins present in the western rift mountains only form a coherent trace trending 265–275° west of our coverage (Rona, 1976). We interpret the off-axis traces of the discontinuity as indicating that it has existed (though not necessarily in its present form) for at least the last 7 Ma. The absence of a trace following a small circle about the pole of relative motion of the African and Northern American plates indicates that a stable transform has not been sustained at this offset in the last 10 Ma (Tucholke and Schouten, 1989).

The 24°51′–25°36′ N segment

This 83-km-long segment has an hourglass morphology (Figure 4a). The shallowest point (3250 m) within the inner floor is found near 25°08′ N. The rift valley and inner floor are narrowest at this latitude. The inner valley is flanked to the west and east by scarps trending 000–015° and 015–025°, respectively. Within our coverage, the western rift mountains consist of two axis-parallel ridges separated by a 200–600-m-deep trough. Both ridges are shallowest and broadest near the waist of the hourglass. The eastern rift mountains consist of four ridges. These ridges are broadest where they are shallowest. The further away the ridges are from the axis, the more elevated and the longer they are. The eastern rift mountains near the 25°36′ N discontinuity are formed by short (5–10 km) faulted blocks. The rift valley is symmetric (profile C–C′) in the saddle area and asymmetric elsewhere. North of the saddle, the east wall rises more rapidly than the west wall (profiles A–A′, B–B′).

Between 24°53′ N and 25°06′ N, the NVZ is associated with subcircular volcanoes aligned along a 015° trend. In the saddle area, the inner floor is devoid of resolvable volcanic edifices that could mark the location of the NVZ. Instead the NVZ appears to occupy the entire narrow inner floor in the saddle area. North of the saddle, the NVZ consists of two *en échelon* volcanic lineaments offset by ~4 km near 25°23′ N (Figure 11). The southern lineament consists of isolated volcanic edifices aligned along a 010° trend, and the northern one of a 20-km-long, 60-m-high ridge striking 016°. These lineaments overlap by 3 km and are separated by a 200-m-deep depression at the small 25°23′ N offset. This minor discontinuity is associated with a change of 6° in the orientation of the NVZ. We classify the NVZ as poorly-developed and robust south and north of 25°23′ N, respectively.

THE 25°36′ N DISCONTINUITY

The axis of the MAR is offset by 11-km in a right-stepping manner near 25°36′ N. There is no evidence for a narrow shear zone between the offset spreading axes. The inter-segment area is characterized by a steep-sided ridge trending 023°. This ridge, labelled A in Figure 4a, is 7-km long and 600-m high. We interpret this ridge as a fault-bounded block which has been isolated from the rift mountains by the migration of the discontinuity.

Prominent bathymetric troughs extend off-axis on both sides of the discontinuity (Figures 4a, 5a). The western trough trends 265°–285°. The eastern trough consists of three distinct basins which form a 105°–125° lineament. Rona (1976) obtained orientations of 112–122° and 270° for the east and west troughs, respectively. The presence of these traces indicate that the offset has persisted through time. Right-stepping jogs of the B–M boundary of 6 and 2 km associated with the west and east traces respectively (Sempéré *et al.*, in prep.), support this interpretation.

THE 25°36′–25°56′ N SEGMENT

The rift valley of this 35-km-long segment is defined by two elevated blocks of small along-axis extent (20–30 km) (Figure 5a). The shallowest point within the inner floor (3400 m) is located near 25°53′ N. The east and west wall of the inner floor trend 350–040° and 015°–040° respectively. All ridges within the rift mountains are widest and highest near their mid-points. The rift valley is symmetric near the segment ends (profiles F–F′, G–G′ and K–K′, Figure 5b). The east wall is more elevated than the west wall near the segment mid-point (profiles H–H′ to J–J′).

The NVZ is located on top of a 5-km-wide ridge which extends between 25°42′ N and 25°55′ N along a strike of 015°. It reaches a minimum depth of 3400 m near 25°53′ N, and depths of 3900 and 3700 m near its south and north ends. Circular volcanic edifices are aligned on the crest of this ridge. The NVZ jogs ~2 km in a left-stepping manner near 25°52′ N (Figure 11). South of 25°42′ N, it veers 35° to the west to form a 7-km-long, 300-m-high ridge which strikes 045°. We classify this NVZ as robust.

THE 25°56′ N DISCONTINUITY

The axis of the MAR is offset by 10 km in a right-stepping manner near 25°56′ N (Figure 5a). The discontinuity is associated with a right-stepping, 14-km offset of the east valley wall near 25°53′ N. The offset NVZs are separated by a 4200-m-deep depression centered near 25°57′ N, 45°01′ W. This basin is flanked to the east by a 016°-trending, fault-bounded ridge which is the south extension of another narrow block. The two blocks are offset by ~1 km near 25°58′ N. This small offset may be indicative of a left-lateral, strike-slip fault between the northern NVZ and the inter-segment basin. Thus, the offset may be accommodated by an extensional basin and a strike-slip fault.

Two basins, centered near 26°01′ N, 45°10′ W and 25°58′ N, 44°47′ W, on the flanks of the discontinuity are part of two lineaments which extend further off-axis along trends 260°–280° and 110–116° (Rona, 1976), and which offset the B–M boundary by 3–4 km (Sempéré *et al.*, in prep.). We interpret these lineaments as the off-axis traces of the discontinuity. We conclude that this offset has existed in the past, and that the strike-slip fault, which may partly accommodate the offset, is a temporary feature because it is not associated with a trace perpendicular to the axis.

THE 25°56′–26°17′ N SEGMENT

This 41-km-long segment, which includes the TAG hydrothermal field (Rona *et al.*, 1986), has been studied in detail by Eberhart *et al.* (1988), Zonenshain *et al.* (1989), Karson and Rona (1990), and Kong *et al.* (1992). The shallowest point along the inner floor lies at a depth of 3550 m near 26°12′ N. At this latitude the inner valley floor is narrowest. The east and west valley walls are associated with axis-facing scarps trending 005°–035° and 010°–030°, respectively (Figure 5a). The rift valley is asymmetric (profiles A–A′ to F–F′, Figure 5b). The west valley wall is generally less elevated and more gently sloping than the east wall, but near the 26°17′ N Discontinuity, the polarity of asymmetry is reversed (profile A–A′). During a submersible transect at 26°08′ N (near profile B–B′), Zonenshain *et al.* (1989) noted that the west valley wall consists of a series of backtilted terraces (5–10°) which form a gentle slope. In contrast, the east valley wall, which has 1 km more relief, consists of a smooth slope with few major faults.

The NVZ is located on a ridge, 18-km long and 100–200-m high, which extends from 25°58′ N to

26°07′ N. The neovolcanic ridge strikes 006° and 031° north and south of 26°01′ N, respectively. North of 26°07′ N the NVZ consists of elongate and circular volcanic edifices aligned in a rough 035° direction.

The 26°17′ N discontinuity

The axis of the MAR is offset by 8 km near 26°17′ N (Figures 5a, 6a). The right-stepping offset is characterized by a ~4400-m-deep, 4-km-wide basin centered near 26°20′ N, 44°42′ W. A zone of strike-slip deformation cannot be identified within the inter-segment area, suggesting that the offset is a non-transform discontinuity. We interpret the rectangular basin within the offset area as an extensional relay zone accommodating the two offset NVZs. Our bathymetric data, as well as those of Rona (1976), indicate that the discontinuity is not associated with off-axis discordant zones and, thus, has not persisted with time.

The 26°17′–26°34′ N segment

The inner floor of this 37-km-long segment forms an hourglass whose waist is located near 26°28′ N (Figure 6a). The inner floor is shallowest (~3700 m) at this latitude. It widens gradually from its minimum width of 6 km to a maximum of 11 km near 26°34′ N and 7 km near 26°17′ N. The west valley wall consists of 200–400-m-high scarps trending 010–030°, the east wall of a 200–600-m-high scarp trending ~020°. A massive rock slide on the east wall of the valley flanks the inner floor near 26°27′ N (Tucholke, 1992). The rift valley is symmetric south of the segment mid-point (profiles K–K′ to M–M′, Figure 6b) but asymmetric north of it. On profile I–I′ and J–J′, the east valley wall is steeper and more elevated than the west one. This higher relief is created by a few large-throw faults. In contrast, the west valley wall consists of several medium-throw faults which create a gently-sloping ramp.

The NVZ is located on top of a ridge which extends for 33 km between 26°19′ N and 26°36′ N along a 013° trend. This ridge is highest (300 m) and widest (3 km) near 26°28′ N, where the inner floor is shallowest. We classify this NVZ as robust. A few small, subcircular volcanic peaks are located on top of this ridge.

The 26°34′ N discontinuity

The axis of the MAR is offset by ~3 km in a right-stepping manner near 26°34′ N (Figure 6a). The two NVZs are separated by a 100-m-deep, 2-km-wide basin. Because there is no evidence for a strike-slip fault linking the NVZs, we interpret this offset as a non-transform discontinuity. The rift mountains flanking the discontinuity are continuous along strike within our coverage, suggesting that the present offset is recent. The B–M boundary is not offset in the vicinity of the discontinuity (Sempéré *et al.*, in prep.). However, bathymetric lows, which form lineaments trending 111° and 264° on the east and west flank, respectively, outside our coverage (Rona, 1976), suggest that the discontinuity has existed in the past.

The 26°34′–26°56′ N segment

The inner floor of this 43-km-long segment has an hourglass morphology (Figure 6a). It is shallowest (3000 m) and narrowest (9 km) near 26°48′ N. It reaches a maximum width of 11 km near 26°37′ N and 27°05′ N. The west wall of the inner valley, which consists of 300–700-m-high scarps trending 010–020°, jogs 6 km in a right-stepping manner near 26°53′ N. The east wall is made up of 200–500-m-high scarps trending 005°–020°. The rift valley is symmetric at the narrowest part of the inner floor (profile F–F′, Figure 6b). North and south of this profile, the west valley wall forms a gentle ramp created by 100–400-m-high faults which bound 2–5-km-wide terraces, while the east wall has a high relief created by faults with cumulative throws on the order of 200–1600 m (profiles D–D′ to H–H′).

The NVZ is robust and poorly-developed south and north of 26°47′ N, respectively. Between 26°33′ N and 26°47′ N, the NVZ lies on top of a 27-km-long ridge trending 005° which veers to an orientation of 030° south of 26°36′ N. North of 26°47′ N, we propose that the NVZ is associated with isolated volcanic cones which lie along a ~010° trend. A ridge consisting of volcanic edifices split in half by axis-parallel faults is present in the inner floor west of the present NVZ. This ridge may correspond to a past expression of the neovolcanic zone (Figure 6c).

The 26°56′ N discontinuity

Near 26°56′ N the NVZ is offset by a 3-km, right-stepping discontinuity (Figure 6a). The NVZ changes orientation by 12° across the offset. The intra-offset area is devoid of obvious structural lineaments

suggesting the presence of a strike-slip fault accommodating the offset. We do not observe structures on the flanks of the offset which could be associated with the past expression of this non-transform discontinuity, indicating that this is either a recent feature, or one which has always been associated with a small offset (< a few km).

The 26°56′–27°09′ N segment

The east and west walls of the inner floor of this 25-km-long segment strike 015° (Figure 6a). The rift valley is asymmetric (profiles A–A′ to C–C′, Figure 6b). The west valley wall forms a gentle ramp created by faults with throws of 100–400 m, while the east wall has a high relief created by faults with cumulative throws of 200–1600 m.

North of 26°56′ N, the NVZ is located on top of a 600-m-high ridge which strikes 017° and extends to about 27°03′ N. Volcanic edifices near the north end of this ridge have been split by a ~1-km-wide, 100-m-deep graben (Figure 6c). North of 27°03′ N, the NVZ corresponds to isolated volcanic cones. We classify the NVZ as robust south of 27°03′ N, and poorly-developed north of this latitude.

The 27°09′ N discontinuity

The MAR axis is offset by a 9-km, right-stepping discontinuity near 27°09′ N (Figures 6a, 7a). The inter-segment area is characterized by a >200-m-high, 5-km-long ridge centered near 27°09′ N, 44°22′ W. This ridge appears to be a volcanic construction. Two >3200-m-deep basins, centered near 27°10′ N, 44°34′ W and 27°09′ N, 44°09′ W, are located on the west and east flank of the spreading center, respectively. These basins may mark the trace of the offset in old seafloor, indicating that the discontinuity is a persistent feature.

The 27°09′–27°43′ N segment

This 64-km-long segment has an hourglass morphology (Figures 7a, b). The shallowest point (3100 m) within the inner floor lies along the NVZ near 27°29′ N. The inner floor is narrowest (6 km) at this latitude, and widens abruptly to a width of 17 and 10 km south and north of the saddle respectively. South of 27°28′ N the west wall of the inner floor consists of 300–800-m-high scarps striking 355°–020° and the east wall of 200–1200-m-high scarps trending 350°–025°. North of 27°28′ N both walls consist of 200–400-m-high scarps trending ~015°. The rift valley is asymmetric (profiles G–G′ to M–M′, Figure 7c). In profiles G–G′ and H–H′ the east flank is somewhat steeper and more elevated than the west flank. The sense of asymmetry is reversed at the segment mid-point (profile I–I′) and south of it (profile J–J′). In the south part of the segment (profiles K–K′ to M–M′), the rift valley appears symmetric.

South of 27°20′ N the NVZ is poorly developed and consists of isolated, volcanic edifices. North of 27°20′ N, the NVZ is robust and located on a 350-m-high ridge which extends to 27°41′ N along an azimuth of 017°.

The 27°43′ N discontinuity

The axis of the MAR is offset by ~9 km near 27°43′ N (Figures 7a, b). The inter-segment area is characterized by two ridges trending 012° and separated by 3 km. The eastern ridge is 150-m high, the western ridge 350-m high. These two ridges appear to be volcanic constructions. The discontinuity corresponds to right-stepping jogs of ~4 km in the rift valley walls. The ridges and troughs of the eastern rift mountains form a staircase pattern of right-stepping jogs, creating a 11-km gradual step between 27°40′ N and 27°47′ N. The east and west B–M boundaries gradually step 6 and 8 km, respectively, near 27°43′ N (Sempéré *et al.*, in prep.). Thus, the discontinuity may have existed prior to 0.72 Ma ago, but it has not left a significant morphologic trace on the flanks of the spreading center.

The 27°43′–28°15′ N segment

This 63-km-long segment has an hourglass morphology (Figures 7a, b). The waist of the hourglass is found near 27°55′ N. The inner valley floor is shallowest (2850 m) at this latitude. The east and west valley walls consist of 200–600-m-high scarps which trend 005–035° and 010–040°, respectively. The western rift mountains are made up of axis-parallel ridges and troughs which coalesce near their mid-points, approximately midway in the segment. The ridges are most elevated and widest near their middle. The rift valley is asymmetric (profiles A–A′ to F–F′, Figure 7c). The east flank is steeper and more elevated than the west flank in the north part of the segment (profiles A–A′ to C–C′) and in our southernmost profile (F–F′). Near the segment mid-point

the west flank is only slightly steeper and more elevated than the east-flank (profiles D–D′ and E–E′).

Between 27°43′ N and 27°55′ N, the NVZ is located on top of a 300-m-high ridge which trends 008°. North of 27°55′ N the NVZ is associated with volcanic constructions which form a 50–200-m-high ridge between 28°01′ N and 28°08′ N. These edifices are loosely aligned along an aximuth of 007°. Near 28°08′ N, the NVZ appears to jog by ~2 km to the left (Figure 11). The NVZ is then associated with isolated volcanic edifices. We classify the NVZ as robust south of 27°55′ N, intermediate between 28°01′ N and 28°08′ N, and poorly-developed elsewhere.

The 28°15′ N discontinuity

Near 28°15′ N, the axis of the MAR is offset 10 km in a right-stepping fashion (Figures 8a, b). A fault-bounded basin with a maximum depth of ~3900 m is located between the offset NVZs. This depression may be an extensional relay basin which accommodates deformation between the offset spreading axes. Two elongate depressions, centered near 28°15′ N, 43°58′ W and 28°13′ N, 44°08′ W, integrate to form a lineament trending 260–290° on the west flank of the MAR. Three elongate basins, centered near 28°13′ N, 43°45′ W, 28°13′ N, 43°43′ W, and 28°09′ N, 43°41′ W, define a lineament trending ~090° in the eastern rift mountains. We interpret these basins as marking the west and east trace of the offset in old seafloor. However, the absence of offsets in the B–M boundary (Sempéré *et al.*, in prep.) indicates that, 0.72 Ma ago, the discontinuity was either small (<3 km), or non-existent.

The 28°15′–28°42′ N segment

This 51-km-long segment has an hourglass morphology (Figures 8a, b). The waist of the hourglass is located near the segment mid-point (28°27′ N). The inner valley floor is shallowest (2900 m) and narrowest (7 km) near 28°25′ N. It widens to 9 km near 28°42′ N and to 18 km near 28°21′ N. The west valley wall consists of 200–400-m-high scarps trending 010–030°. South of 28°21′ N, the east wall corresponds to a 800–1000-m-high scarp which trends 025°. The east flank of the rift valley is more elevated and steeper than the west one (profiles K–K′ to Q–Q′, Figure 8c). The topography of the eastern rift mountains is created by a few, large-throw, axis-facing faults. In contrast, the west flank is made up of 1–5-km-wide, fault-bounded terraces which progressively step up in the rift mountains.

The NVZ is located on top of a 200–400-m-high ridge which extends for 40 km between 28°15′ N and 28°36′ N. We classify this NVZ as robust. The NVZ trends 010° between its north terminus and 28°20′ N at which point it veers to a 028° orientation. The NVZ is topped by subcircular volcanic edifices. Near 28°36′ N, the NVZ is offset ~1 km in a left-stepping manner onto a 300-m-high ridge which extends for 8 km along a strike of 022° (Figure 11).

The 28°42′ N discontinuity

The axis of the MAR steps to the right by 9 km near 28°42′ N (Figures 8a, b). The discontinuity corresponds to right-stepping jogs of 11 and 6 km of the west and east valley walls, respectively. The offset zone is characterized by the two ~E–W escarpments, with opposite dip directions, which bound the north and south segments. Two basins, centered near 28°37′ N, 43°51′ W and between 44°12′ W and 44°05′ W near 28°38′ N, integrate to form a 260–280°-trending lineament on the west flank of the axis. Four basins are located in the rift mountains east of the discontinuity. We infer that the discontinuity has persisted with time from the existence of these off-axis traces.

The 28°42′–28°51′ N segment

The inner floor of this 22-km-long segment is located within a wide rhombocasm (Figures 8a, b). The 800–1200-m-high west valley wall trends 010° and 055° south and north of 28°50′ N, respectively. The 500–1200-m-high east wall is more linear and trends 035°. The width of the inner floor varies between 11 and 16 km. The rift valley is asymmetric (profiles H–H′ to J–J′, Figure 8c). The sense of asymmetry changes along strike: near the south end of the segment, the east wall is the more elevated, whereas the western wall dominates the middle and north end.

We interpret the NVZ as lying along a 19-km-long, 100–200-m-high band of coalescing, elongate volcanic edifices which strikes ~038°, an azimuth markedly oblique to the orientation of the NVZ within other segments (~010°). We classify the NVZ as intermediate to poorly-developed.

THE 28°51′ N DISCONTINUITY

The axis of the MAR is offset by 9 km to the right near 28°51′ N (Figures 8a, b). The inter-segment area is characterized by two steep-sided ridges, labelled A and B in Figure 8b, separated by ~2 km. Ridge A is 450-m high and trends 032°. Ridge B is 300-m high and trends 007°. Three >3200-m-deep, axis-parallel basins define a lineament trending 265–290° on the west flank of the discontinuity. Two 3200-m-deep basins lie along an azimuth of 085–115° on the east flank of the offset. We interpret these lineaments as marking the off-axis traces of the discontinuity. The west B–M boundary is offset in a right-stepping manner by about 4 km near 28°59′ N, but there is no significant offset in the east B–M boundary (Sempéré *et al.*, in prep.).

THE 28°51′–29°23′ N SEGMENT

This 62-km-long segment has an hourglass morphology (Figures 8a, b). The inner floor is narrowest (5 km) at 29°04′ N near the segment mid-point. The shallowest depths within the inner valley floor (~3100 m) are found between 29°02′ N and 29°09′ N. The west valley wall, which is made up of 100–400-m-high scarps trending 010–040°, abuts against a >1000-m-high, E–W escarpment near 29°25′ N. The east wall consists of 200–400-m-high scarps trending 005–025° south of 29°15′ N, and of 500–800-m-high scarps striking 015–040° north of 29°15′ N. The east and west valley walls are more continuous and less elevated near the mid-point of the segment. The rift valley is asymmetric (profiles A–A′ to G–G′, Figure 8c). North of 29°05′ N, the east wall is more elevated and steeper than the west wall (profiles A–A′ to D–D′). The converse is true on profile G–G′, while profiles E–E′ and F–F′ display a symmetric rift structure. The rift mountain ridges are widest and highest near the waist of the hourglass rift valley.

The NVZ is located on a 300-m-high ridge between 28°52′ N and 29°15′ N. The NVZ trends 010° north of 28°55′ N, but veers to an orientation of 026° south of this latitude. The NVZ is offset by a ~2-km right step near 29°14′ N (Figure 11). The two offset limbs overlap by ~3 km and are separated by a 100-m-deep depression. North of 29°14′ N, the NVZ is associated with a band of volcanic edifices which form a 011° lineament. We classify the NVZ as robust and poorly-developed south and north of 29°15′ N, respectively.

THE 29°23′ N DISCONTINUITY

The axis of the MAR is offset by 17 km near 29°23′ N (Figures 8a, 8b, 9a). This non-transform discontinuity is right-stepping. The two offset rift valleys overlap by ~15 km. They are separated by a fault-bounded block trending ~020°. The inter-segment block reaches a minimum depth of ~2200 m near 29°25′ N, 42°59′ W, 1800 and 1500 m above the deepest portions of the adjacent northern and southern rift valleys, respectively.

Five isolated 3200–3300-m-deep basins (C1–C5, Figure 8b) define a lineament trending 265–300° on the west flank of the discontinuity. Two basins, centered near 29°18′ N, 42°45′ W and 29°16′ N, 42°39′ W, integrate to form a 095–115°-trending lineament on the east flank. We interpret these two discordant zones as marking the off-axis traces of the discontinuity. The B–M boundary is offset in a right-stepping manner by 9 and 8 km on the west and east flanks of the discontinuity, respectively (Sempéré *et al.*, in prep.).

THE 29°23′–29°49′ N SEGMENT

This 49-km-long segment has an hourglass morphology (Figure 9a). The inner floor, which shoals northward between the two bounding discontinuities, is narrowest near 29°37′ N (7 km). It reaches maximum widths of 10 and 14 km near 29°22′ N and 29°45′ N. The west valley wall trends ~013°. The east wall is made up of 200–900-m-high scarps trending 007–020°. The rift valley is asymmetric away from the segment mid-point (Figure 9b). The east rift valley wall is made up of a single, or a few closely-spaced, axis-facing faults with a cumulative throw of several hundred meters, while the west valley wall consists of a gentler staircase pattern of faults.

The NVZ is located on top of a 33-km-long ridge between 29°31′ N and 29°48′ N. The ridge is shallowest (2900 m) near 29°45′ N. The NVZ jogs to the right by <1 km near 29°38′ N. South of 29°31′ N the NVZ is associated with isolated, volcanic edifices aligned along an azimuth of 015°. We classify the NVZ as robust and poorly-developed north and south of 29°31′ N, respectively.

THE 29°49′ N DISCONTINUITY

The axis of the MAR is offset by ~1 km near 29°49′ N (Figure 9a). This left-stepping offset is not located at a local depth maximum. The inter-segment area corresponds to a 50-m-deep depression. The discontinuity is not associated with recognizable off-axis traces. The small size of the offset and the continuity of gravity anomalies across it (Lin *et al.*, 1990) indicate that the offset may only be a minor jog in the MAR axis. However, we consider this small offset to be important because it separates two sections of the MAR with markedly distinct morphologies.

THE 29°49′ N-ATLANTIS SEGMENT

Because of its close relationship to the Atlantis Fracture Zone, the morphology of this short segment is discussed in our study of the Atlantis Transform (Zervas *et al.*, in prep).

THE ATLANTIS-30°33′ N SEGMENT

The width and depth of the rift valley of this 64-km-long segment vary from 5 km and 4050 m at 30°05′ N to 17 km and 2800 m at 30°30′ N (Figure 10a). The shallowest point (2700 m) within the inner floor occurs near 30°31′ N. The west valley wall, which trends 015–025°, jogs to the left by 10 km near 30°25′ N. The 600–1400-m-high east valley wall strikes 010–015° between the transform and 30°18′ N. Between 30°26′ N and 30°32′ N, it consists of >500-m scarps trending 020–060° which create a 6-km, right-stepping jog. The rift valley is asymmetric. South of 30°25′ N, the west flank of the rift valley is steeper than the east flank (profiles D–D′ to H–H′, Figure 10b) but, north of 30°25′ N, the sense of asymmetry is reversed (profiles A–A′ to C–C′).

South of 30°08′ N we do not observe any volcanic features which could be associated with the NVZ. North of 30°08′ N, the NVZ is associated with isolated, volcanic edifices. North of 30°19′ N, the NVZ lies on top of a ridge. Between 30°27′ N and 30°32′ N the NVZ consists of two 015°-trending ridges, scattered by small volcanic peaks, which lie at an average depth of ~2800 m. These two ridges form a 400-m-high, 7-km-wide construction. We classify the NVZ as poorly-developed south of 30°19′ N and robust north of this latitude.

THE 30°33′ N DISCONTINUITY

The axis of the MAR is offset by ~8 km near 30°33′ N. The nature of this right-stepping discontinuity is not well defined due to the position of the offset at the edge of our survey area. We infer that the NVZ in the segment north of the offset corresponds to a 016°-trending ridge (Figure 10a). The offset spreading axes are separated by an elongate depression trending 025°. Because there is no evidence for a strike-slip fault linking the offset NVZs, we interpret the discontinuity as non-transform in nature.

References

Argus, D. F., Gordon, R. G., DeMets, C., and Stein, S., 1989, Closure of the Africa-Eurasia-North-America plate motion circuit and tectonics of the Gloria fault, *J. Geophys. Res.* **94**, 5585–5603.

Ballard, R. D. and T. H. van Andel, 1977, Morphology and tectonics of the inner rift valley at lat 36°50′ N on the Mid-Atlantic Ridge, *Geol. Soc. Am. Bull.* **88**, 507–530.

Barone, A. M. and Ryan, W. B. F., 1988, Along-axis variations within the plate boundary zone of the Southern segment of the Endeavour Ridge, *J. Geophys. Res.* **93**, 7856–7868.

Bergman, E. A. and Solomon, S. C., 1990, Earthquake swarms on the Mid-Atlantic Ridge: Products of magmatism or extensional tectonics? *J. Geophys. Res.* **95**, 4943–4965.

Bosworth, W., 1985, Geometry of propagating continental rifts, *Nature* **316**, 625–627.

Brown, J. R. and Karson, J. A., 1988, Variations in axial processes on the Mid-Atlantic Ridge: The median valley of the MARK area, **10**, 109–138.

Brown, H. S., Sempéré, J.-C., Rommevaux, C., and Patriat, P., 1990, Three-Dimensional Inversion of the Magnetic Field along the Mid-Atlantic Ridge: Evolution of the Plate Boundary between 28° N and 29° N in the last 10 Ma (abstract), *EOS Trans AGU* **71**, 1572.

Brozena, J., 1986, Temporal and spatial variability of seafloor spreading processes in the northern South Atlantic, *J. Geophys. Res.* **91**, 497–510.

Brozena, J. and Chayes, D., 1988, A sea Beam study of the Mid-Atlantic Ridge, 15°–17° S (abstract), *Eos Trans. AGU* **69**, 1494.

Carbotte, S., Welch, S. M., and Macdonald, K. C., 1991, Spreading rates, rift propagation, and fracture zones offset histories during the past 5 My on the Mid-Atlantic Ridge; 25°–27°30′ S and 31°–34°30′ S, *Mar. Geophys. Res.* **13**, 51–80.

Choukroune, P., Francheteau, J., and LePichon, X., 1978, In situ structural observations along Transform Fault A in the FAMOUS area, *Bull. Geol. Soc. Am.* **88**, 1013–1029.

Cormier, H. H., Detrick, R. S., and Purdy, G. M., 1984, Anomalously thin crust in oceanic fracture zones: New seismic constraints from the Kane fracture zone, *J. Geophys. Res.* **89**, 10249–10266.

Crane, K. and Ballard, R. D., 1981, Volcanics and structure of the FAMOUS Narrowgate rift: Evidence for cyclic evolution, *J. Geophys. Res.* **86**, 5112–5124.

Crane, K., 1985, The spacing of rift axis highs: Dependence upon

diapiric processes in the underlying asthenosphere? *Earth Planet, Sci. Lett.* **72**, 405–414.

Detrick, R. S., Mudie, J. D., Luyendyk, B. P., and Macdonald, K. C., 1973, Near-bottom observations of an active transform fault (Mid-Atlantic Ridge at 37° N), *Nature* **246**, 59–61.

Detrick, R. S., Cormier, M. H., Prince, R. A., Forsyth, D. W., and Ambos, E. L., 1982, Seismic constraints on the crustal structure of the Vema fracture zone, *J. Geophys. Res.* **87**, 10599–10612.

Dick, H. J. B., 1989, Abyssal peridotites, very slow spreading ridges and ocean ridge magmatism, In A. D. Saunders and M. J. Norry (eds.), Magmatism in the Ocean Basins *Geological Society Special Publication* **42**, 71–105.

Eberhart, G. L., Rona, P. A., and Honnorez, J., 1988, Geologic controls of hydrothermal activity in the Mid-Atlantic Ridge rift valley: Tectonics and volcanics, *Mar. Geophys. Res.* **10**, 233–259.

Ebinger, C. J., 1989a, Tectonic development of the western branch of the East African rift system, *Geol. Soc. Am. Bull.* **101**, 885–903.

Ebinger, C. J., 1989b, Geometric and kinematic development of border faults and accommodation zones, Kivu-Rusizi rift, Africa, *Tectonics* **8**, 117–133.

Ebinger, C. J., Deino, A. L., Drake, R. E., and Teisha, A. L., 1989, Chronology of volcanism and rift basin propagation: Rungwe volcanic province, East Africa, *J. Geophys. Res.* **94**, 15785–15803.

Fox, P. J. and Gallo, D. G., 1984, A tectonic model for ridge-transform-ridge plate tectonics: Implications for the structure of oceanic lithosphere, *Tectonophysics* **104**, 205–242.

Fox, P. J., Grindlay, N. R., Macdonald, K. C., Bicknell, J. D., and Forsyth, D. W., 1985, The morphotectonic character of the Mid-Atlantic Ridge between 31–34° S: Implications for plate accretion (abstract), *Eos Trans. AGU* **66**, 1078.

Fox, P. J. and Gallo, D. G., 1986, The geology of north Atlantic transform plate boundaries and their aseismic extensions, In P. Vogt and B. Tucholke (eds.), Decade of North American Geology, vol. M, Geological Society of America, Boulder, Colo., pp. 157–172.

Fox, P. J., Grindlay, N. R., and Macdonald, K. C., 1991, The Mid-Atlantic Ridge (31°–34° S): Temporal and spatial variations of accretionary processes, *Mar. Geophys. Res.* **13**, 1–20.

Gente, P., Aslanian, D., Campan, A., Cannat, M., Ceuleneer, G., Deplus, C., Durand, C., Laverne, C., Leau, H., Maia, M., Marion, E., Mével, C., Pockalny, R., and Seyler, M., 1991, Geometry of past and present-day segmentation of the Mid-Atlantic Ridge south of Kane fracture zone (abstract), *EOS Trans. AGU* **72**, 476–477.

Gibbs, A. D., 1984, Structural evolution of extensional basin margins, *J. Geol. Soc. Lond.* **141**, 609–620.

Glenn, M. F., 1976, Multi-narrow beam sonar systems, Proc. MTS-IEEE Oceans '76 Conf., **8**, D1–D2.

Goud, M. R. and Karson, J. A., 1985, Tectonics of short-offset, slow-slipping transform zones in the FAMOUS area, Mid-Atlantic Ridge, *Mar. Geophys. Res.* **7**, 489–514.

Grindlay, N. R., Fox, P. J., and Macdonald, K. C., 1991, Second-order ridge axis discontinuities in the south Atlantic: Morphology, structure, and evolution, *Mar. Geophys. Res.* **13**, 21–50.

Harper, G. D., 1988, Episodic magma chambers and amagmatic extension in the Josephine ophiolite, *Geology* **16**, 831–834.

Johnson, G. L. and Vogt, P. R., 1973, Mid-Atlantic Ridge from 47° to 51° N, *Geol. Soc. Am. Bull.* **84**, 3443–3462.

Kappel, E. S. and Ryan, W. B. F., 1986, Volcanic episodicity and a non-steady state rift valley along northeast Pacific spreading centers: Evidence from SeaMARC I, *J. Geophys. Res.* **91**, 13925–13940.

Karson, J. A. and Dick, H. J. B., 1983, Tectonics of ridge transform intersections at the Kane fracture zone, *Mar. Geophys. Res.* **6**, 51–98.

Karson, J. A., Thompson, G., Humphris, S. E., Edmond, J. M., Bryan, W. B., Brown, J. R., Winters, A. T., Pockalny, R. A., Casey, J. R., Campbell, A. C., Klinkhammer, G., Palmer, M., Kinzler, R. J., and Sulanowska, M. M., 1987, Along-axis variations in seafloor spreading in the MARK area, *Nature* **328**, 681–685.

Karson, J. A. and Curtis, P. C., 1989, Tectonic and magmatic processes in the Eastern Branch of the East African Rift and implications for magmatically active continental rifts, *J. of African Earth Sciences* **8**, 431–453.

Karson, J. A. and Rona, P. A., 1990, Block-tilting, transfer faults and structural control on magmatic activity and hydrothermal processes in the TAG area, Mid-Atlantic Ridge 26° N, *Geol. Soc. Am. Bull.* **102**, 1635–1645.

Karson, J. A., 1990, Accommodation zones and transfer faults: Integral components of Mid-Atlantic Ridge extensional systems, In A. Nicolas and Tj. Peters (eds.), *Proceedings of the Symposium on Oceanic Lithosphere and the Oman Ophiolite*, in press.

Kong, L. S. L., Detrick, R. S., Fox, P. J., Mayer, L. A., and Ryan, W. B. F., 1988, The morphology and tectonics of the MARK area from Sea Beam and Sea MARC I observations (Mid-Atlantic Ridge 23° N), *Mar. Geophys. Res.* **10**, 59–90.

Kong, L. S. L., Solomon, S. C., and Purdy, G. M., 1992, Microearthquake characteristics of a mid-ocean ridge along-axis high, *J. Geophys. Res.* **97**, 1659–1685.

Kong, L. S. L., Purdy, G. M., and Solomon, S. C., 1991b, Along-axis variations in crustal structure on the Mid-Atlantic Ridge near 26° N, *J. Geophys. Res.*, (submitted).

Langmuir, C. H., Bender, J. F., and Batiza, R., 1986, Petrologic and tectonic segmentation of the East Pacific Rise, 5°30′ N–14°30′ N, *Nature* **322**, 422–429.

LeDouaran, S. and Francheteau, J., 1981, Axial depth anomalies from 10 to 50° north along the Mid-Atlantic Ridge: correlation with other mantle properties, *Earth Planet. Sci. Lett.* **54**, 29–47.

Lin, J., Purdy, G. M., Schouten, H., Sempéré, J.-C., and Zervas, C., 1990, Evidence from gravity data for focused magmatic accretion along the Mid-Atlantic Ridge, *Nature* **344**, 627–632.

Lin, J. and Bergman, E. A., 1991, Rift grabens, seismicity, and volcanic segmentation of the Mid-Atlantic Ridge: Kane to Atlantis Fracture Zones (abstract), *EOS Trans. AGU* **71**, 1572.

Lin, J. and Phipps Morgan, J., 1992, The spreading rate dependence of 3-D Mid-ocean ridge structure, *Geophys. Res. Lett.* **19**, 13–16.

Lonsdale, P., 1983, Overlapping rift zones at the 5.5° S offset of the East Pacific Rise, *J. Geophys. Res.* **88**, 9393–9406.

Lonsdale, P., 1985, Non transform offsets of the Pacific-Cocos plate boundary and their trace on the rise flank, *Geol. Soc. Am. Bull.* **96**, 313–327.

Lonsdale, P., 1989, The rise flank trails left by migrating offsets of the equatorial East Pacific Rise axis, *J. Geophys. Res.* **94**, 713–743.

Lonsdale, P., 1989b, Segmentation of the Pacific-Nazca spreading center, 1° N–20° S, *J. Geophys. Res.* **94**, 12197–12225.

Louden, K. E. and Forsyth, D. W., 1982, Crustal structure and isostatic compensation near the Kane fracture zone from topography and gravity measurements-I. Spectral analysis approach, *Geophys. J. R. Astr. Soc.* **68**, 725–750.

Luyendyk, B. P. and Macdonald, K. C., 1977, Physiography and structure of the inner floor of the FAMOUS rift valley: observations with a deeply towed instrument package, *Geol. Soc. Am. Bull.* **88**, 648–663.

Macdonald, K. C. and Luyendyk, B. P., 1977, Deep-tow studies of the structure of the Mid-Atlantic Ridge crest near lat. 37° N, *Geol. Soc. Am. Bull.* **88**, 621–636.

Macdonald, K. C., Sempéré, J.-C., and Fox, P. J., 1984, The East Pacific Rise from the Siqueiros to the Orozco fracture zone: Along strike continuity of the neovolcanic zone and the structure and evolution of overlapping spreading centers, *J. Geophys. Res.* **89**, 6049–6069.

Macdonald, K. C., Sempéré, J.-C., and Fox, P. J., 1986, Reply: The debate concerning overlapping spreading centers and mid-ocean ridge processes, *J. Geophys. Res.* **91**, 10501–10511.

Macdonald, K. C., 1986, The crest of the Mid-Atlantic Ridge: Models for crustal generation processes and tectonics, In P. Vogt and B. Tucholke (eds.), *Decade of North American Geology: The Western North Atlantic Region*, vol. M., Geological Society of America, Boulder, Colo., pp. 51–68.

Macdonald, K. C., Fox, P. J., Perram, L. J., Eisen, M. F., Haymon, R. M., Miller, S. P., Carbotte, S. M., Cormier, M.-H., and Shor, A. N., 1988, A new view of the mid-ocean ridge from the behaviour of the ridge axis-discontinuities, **335**, 217–225.

McCarthy, J., Mutter, J. C., Morton, J. L., Sleep, N. H., and Thompson, G. A., 1988, Relic magma chamber structures preserved within the Mesozoic North Atlantic crust? *Geol. Soc. Am. Bull.* **100**, 1423–1436.

Melson, W. G. and O'Hearn, T., 1986, 'Zero-age' variations in the composition of abyssal volcanic rocks along the axial zone of the Mid-Atlantic Ridge, In P. Vogt and B. Tucholke (eds.), *Decade of North American Geology: The western north Atlantic Region*, Vol. M., Geological Society of America, Boulder, Colo., pp. 117–136.

Miller, S. P., 1977, The validity of the geological interpretation of marine magnetic anomalies, *Geophys. J. R. Astron. Soc.* **50**, 1–21.

Minshull, T. A., White, R. S., Mutter, J. C., Buhl, P., Detrick, R. S., Williams, C. A., and Morris, E., 1991, Crustal structure at the Blake Spur Fracture Zone from expanding spread profiles, *J. Geophys. Res.* **96**, 9955–9984.

Morley, C. K., Nelson, R. A., Patton, T. L., and Munn, S. G., 1990, Transfer zones in the East African Rift system and their relevance to hydrocarbon exploration in rifts, *Am. Ass. Petrol. Geol.* **74**, 1234–1253.

Morris, E. and Detrick, R. S., 1991, Three-dimensional analysis of gravity anomalies in the MARK area, Mid-Atlantic Ridge 23° N, *J. Geophys. Res.* **96**, 4355–4366.

Mutter, J. C., Detrick, R. S., and the NAT Study Group, 1984, Multichannel seismic evidence for anomalously thin crust at Blake-Spur fracture zone, *Geology* **12**, 534–537.

Mutter, J. C. and North Atlantic Transect Study Group, 1985, Multichannel seismic images of the oceanic crust's internal structure: Evidence for a magma chamber beneath the Mesozoic Mid-Atlantic Ridge, *Geology* **13**, 629–632.

Needham, H. D., Auffret, G. A., Ballu, V., Beuzart, P., Dauteuil, O., Detrick, R., Dubois, J., Carré, D., Lance, S., Langmuir, C., LeDrezen, E., Normand, A., Renard, V., Voisset, M., and Bougault, H., 1991, The crest of the Mid-Atlantic Ridge between 40° N and 15° N: Very broad swath mapping with the EM12 echosounding system (abstract), *EOS Trans. AGU* **72**, 470.

Nicolas, A., 1985, Novel type of oceanic crust produced during continental rifting, *Nature* **315**, 112–115.

North Atlantic Transect Study Group, 1985, North Atlantic Transect: A wide-aperture, two-ship multichannel seismic investigation of the oceanic crust, *J. Geophys. Res.* **90**, 10321–10341.

Norrell, G. T. and Harper, G. D., 1988, Detachment faulting and amagmatic extension at mid-ocean ridges: the Josephine ophiolite as an example, *Geology* **16**, 827–830.

Parmentier, E. M. and Forsyth, D. W., 1985, Three-dimensional flow beneath a slow spreading ridge axis: A dynamic contribution to the deepening of the median valley toward fracture zones, *J. Geophys. Res.* **90**, 678–684.

Parmentier, E. M. and Phipps Morgan, J., 1990, The spreading rate dependence of three-dimensional spreading center structure, *Nature* **348**, 325–328.

Patriat, P., Deplus, C., Rommevaux, C., Sloan, H., Hunter, P., and Brown, H. S., 1990, Evolution of the segmentation of the Mid-Atlantic Ridge between 28° N and 29° N in the last 10 Ma: Preliminary results from the SARA cruise (R/V Jean Charcot, May 1990) (abstract), *EOS Trans AGU* **71**, 1629.

Phillips, J. D. and Fleming, H. S., 1977, Multibeam sonar study of the Mid-Atlantic Ridge rift valley 36°–37° N, *Geol. Soc. Am. Bull.* **88**, 1–5.

Phipps Morgan, J., Parmentier, E. M., and Lin, J., 1987, Mechanisms for the origin of mid-ocean ridge axial topography: Implications for the thermal and mechanical structure of accreting plate boundaries, *J. Geophys. Res.* **92**, 12823–12836.

Pockalny, R. A., Detrick, R. S., and Fox, P. J., 1988, Morphology and tectonics of the Kane transform from Sea Beam bathymetry data, *J. Geophys. Res.* **93**, 3179–3193.

Pollard, D. D. and Aydin, A., 1984, Propagation and linkage of oceanic ridge segments, *J. Geophys. Res.* **89**, 10017–10028.

Prévot, M., Lecaille, A., and Hékinian, R., 1979, Magnetism of the Mid-Atlantic Ridge crest near 37° N from FAMOUS and DSDP results: A review, In M. Talwani, C. G. Harrison, and D. E. Hayes (eds.), *Deep Sea Drilling Results in the Atlantic Ocean*, Maurice Ewing Series 2, AGU, Washington D.C., pp. 431.

Prince, R. A. and Forsyth, D. W., 1988, Horizontal extent of anomalously thin crust near the Vema fracture zone from the three-dimensional analysis of gravity anomalies, *J. Geophys. Res.* **93**, 8051–8063.

Purdy, G. M. and Detrick, R. S., 1986, The crustal structure of the Mid-Atlantic Ridge at 23° N from seismic refraction studies, *J. Geophys. Res.* **91**, 3739–3762.

Purdy, G. M., Sempéré, J.-C., Schouten, H., Dubois, D., and Goldsmith, R., 1990, Bathymetry of the Mid-Atlantic Ridge, 24°–31° N: A Map Series, *Mar. Geophys. Res.* **12**, 247–252.

Rabinowicz, M., Phipps Morgan, J., Ceuleneer, G., and Rosenberg, C., 1990, The interaction of small scale convection with 3-D upwelling beneath a spreading center (abstract), *EOS Trans. AGU* **71**, 1637.

Ramberg, I. B., Gray, D. F., and Raynolds, R. G. H., 1977, Tectonic evolution of the FAMOUS area of the Mid-Atlantic Ridge, lat. 35°50′ N to 37°20′ N, *Geol. Soc. Am. Bull.* **88**, 609–620.

Ramberg, I. B. and van Andel, T. H., 1977, Morphology and tectonic evolution of the rift valley at lat 36°30′ N, Mid-Atlantic Ridge, *Geol. Soc. Am. Bull.* **88**, 577–586.

Reid, I. and Macdonald, K. C., 1973, Microearthquake study of the Mid-Atlantic Ridge near 37° N using sonobuoys, *Nature* **246**, 88–90.

Renard, V. and Allenou, J. P., 1979, Sea Beam, multibeam echo-sounding in 'Jean Charcot', *Int. Hydrogr. Rev.* **56**, 35–67.

Rona, P. A., 1976, Asymmetric fracture zones and seafloor spreading, *Earth Planet. Sci. Lett.* **30**, 109–116.

Rona, P. A., Harbison, R. N., Bussinger, B. G., Scott, R. B., and Natwalk, A. J., 1976, Tectonic fabric and hydrothermal activity of the Mid-Atlantic Ridge crest (lat 26° N), *Geol. Soc. Am. Bull.* **87**, 661–674.

Rona, P. A. and Gray, D. F., 1980, Structural behavior of fracture zones symmetric and asymmetric about a spreading axis: Mid-Atlantic Ridge crest (lat 23° N to 27° N), *Geol. Soc. Am. Bull.* **91**, 485–496.

Rona, P. A., Klinkhammer, G., Nelsen, T. A., Trefry, J. H., and Elderfield, H., 1986, Black smoker, massive sulfides and vent biota at the Mid-Atlantic Ridge, *Nature* **321**, 33–37.

Rosendahl, B. R., 1987, Architecture of continental rifts with special reference to East Africa, *Ann. Rev. Earth Planet. Sci.* **15**, 445–503.

Schilling, J.-G., 1986, Geochemical and isotopic variation along the Mid-Atlantic Ridge axis from 79° N to 0° N, In P. Vogt and B. Tucholke (eds.), *Decade of North American Geology: The Western North Atlantic Region*, Vol. M., Geological Society of America, Boulder, Colo., pp. 137–156.

Schouten, H. and White, R. S., 1980, Zero-offset fracture zones, *Geology* **8**, 175–179.

Schouten, H. and Klitgord, D. K., 1982, The memory of the accreting plate boundary and the continuity of fracture zones, *Earth Planet. Sci. Lett.* **59**, 255–266.

Schouten, H., Klitgord, K. D., and Whitehead, J. A., 1985, Segmentation of mid-ocean ridges, *Nature* **317**, 225–229.

Schouten, H., Dick, H. J. B., and Klitgord, K. D., 1987, Migration of mid-ocean ridges, *Nature* **326**, 835–839.

Searle, R. C. and Laughton, A. S., 1977, Sonar studies of the Mid-Atlantic Ridge and Kurchatov Fracture Zone, *J. Geophys. Res.* **82**, 5313–5328.

Searle, R. C., 1986, GLORIA investigations of oceanic fracture zones: comparative study of the transform fault zones, *J. Geol. Soc. Lond.* **143**, 743–756.

Sempéré, J.-C. and Macdonald, K. C., 1986, Overlapping spreading centers: Implications from crack growth simulation by the displacement discontinuity method, *Tectonics* **5**, 151–163.

Sempéré, J.-C., Purdy, G. M., and Schouten, H., 1990, The segmentation of the Mid-Atlantic Ridge between 24° N and 30°40′ N, *Nature* **344**, 427–431.

Sempéré, J.-C., 1991, Tectonic variations along the axis of the Mid-Atlantic Ridge: Observations and finite-element modelling (abstract), *EOS Trans. AGU* **72**, 471.

Sinha, M. C. and Louden, K. E., 1983, The Oceanographer fracture zone – I. Crustal structure from seismic refraction studies, *Geophys. J. R. Astr. Soc.* **75**, 713–736.

Tamsett, D. and Searle, R., 1988, Structure and development of the mid-ocean ridge plate boundary in the Gulf of Aden: Evidence from GLORIA side-scan sonar, *J. Geophys. Res.* **93**, 3157–3178.

Tucholke, B. E. and Schouten, H., 1989, Kane Fracture Zone, *Mar. Geophys. Res.* **10**, 1–40.

Tucholke, B. E., 1992, Massive submarine rock slide on the rift valley of the Mid-Atlantic Ridge, *Geology* **20**, 129–132.

Tyce, R. C., 1986, Deep seafloor mapping systems – A review, *MTS Journal* **20**, 4–16.

Vogt, P. R., Cande, S., Fox, P. J., and Grindlay, N. R., 1987, Detailed investigation of a flowline corridor in the south Atlantic: Part I – Mid-Atlantic Ridge crestal area (abstract), *Eos Trans. AGU* **68**, 1491.

White, R. S. and Matthews, D. R., 1980, Variations in oceanic upper crustal structure in a small area of the northeastern Atlantic, *Geophys. J. Roy. Astr. Soc.* **61**, 401–431.

White, R. S., 1984, Atlantic oceanic crust: seismic structure of a slow-spreading ridge, In I. G. Gass, S. J. Lippard and A. W. Shelton (eds.), *Ophiolites and Oceanic Lithosphere*, Geol. Soc. London, *Special Publication* **13**, 101–111.

Whitehead, J., Dick, H. J. B., and Schouten, H., 1984, A mechanism for magmatic accretion under spreading centers, *Nature* **312**, 146–148.

Zervas, C. E., Lin, J., and Rona, P., 1990, Asymmetric V-shaped gravity stripes at the Mid-Atlantic Ridge 26° N (abstract), *Eos Trans. AGU* **71**, 1572.

Zonenshain, L. P., Kuzmin, M. I., Lisitsin, A. P., Bogdanov,, Y. A., and Baranov, B. V., 1989, Tectonics of the Mid-Atlantic Rift valley between the TAG and MARK areas (26–24° N): Evidence for vertical tectonism, *Tectonophysics* **159**, 1–23.